Sustainable Energy, Grids and Networks 47 (2026) 102431

Contents lists available at ScienceDirect

Sustainable Energy, Grids and Networks

journal homepage: www.elsevier.com/locate/segan

Optimal storage utilization and reliability assessment in AC/DC microgrids with environmentally driven renewable integration

Salar Moradi *, Salvatore Favuzza, Mariano Giuseppe Ippolito, Andrea Marletta, Giulia Marcon, Fabio Massaro, Gaetano Zizzo

Engineering Department, University of Palermo, Building 9, Palermo, Italy

ARTICLE INFO

Keywords:
Optimal power dispatch
State of charge
Renewables
AC/DC microgrids
Reliability
Bootstrap
Time series

ABSTRACT

This paper presents a day-ahead optimal power dispatch framework for grid-connected AC/DC microgrids integrating Renewable Energy Sources (RESs) and Battery Energy Storage Systems (BESSs), aiming at power supply improvement in off-grid mode. The optimization minimizes energy imported from the main grid while maximizing the state of charge (SoC) of BESSs. Renewable power outputs were modeled for various scenarios related to external conditions using time series analysis of historical environmental data, such as wind speed, solar irradiation, and temperature. The energy management strategies were evaluated under these scenarios, including transitions to islanded mode triggered by grid faults. In grid-connected mode, a new adaptive SoC-based charging/discharging strategy is incorporated into the objective function. This strategy not only minimizes the total operation cost but also ensures that storage systems maintain sufficient energy to supply critical loads during islanded mode while reducing the frequency of switching between charging and discharging operation modes. In islanded operation, two reliability indices were introduced to measure resilience under different scenarios. In both on-grid and off-grid operation modes, a SoC balancing strategy is considered to prolong the lifespan of the BESSs. The application of the proposed model to three case studies under various energy scenarios is programmed and simulated in Python. The findings indicate that: (1) the SoC of storage systems may change depending on the season and energy scenario; (2) fast SoC balancing convergence is possible; and (3) the worst energy scenarios can sometimes lead to greater resilience, although they may also result in lower average reliability overall.

1. Introduction

Unlike traditional power systems, due to non-dispatchable power sources such as Photovoltaic (PV) and Wind Turbine (WT), and controlled power electronic interfaces, microgrids have some challenges in the context of Energy Management System (EMS), planning, reliability, control, and protection, among others, especially in islanded operation mode [1–3]. Among these challenges, day-ahead power allocation and energy management at the tertiary control level play a crucial role in ensuring economical operation, efficient utilization of renewable resources, and secure power supply during transitions between grid-connected and islanded operating modes. Unlike primary and secondary control strategies, which operate on fast dynamic timescales for voltage and frequency regulation, tertiary-level energy management focuses on optimal power dispatch and scheduling over longer operational horizons. This paper aims to address a tertiary-level control framework in EMS context, providing optimal power dispatch in AC/DC microgrids in on-grid mode while considering power supply security constraints in off-grid operation to enhance resiliency during islanding mode. In this algorithm, the program seeks to achieve efficient utilization of storage systems, ensuring the most resilient operation in off-grid mode and an increased BESS lifetime. In addition, different scenarios for RES output power, reflecting unpredictable environmental parameters, are analyzed. Therefore, the literature below evaluates the state-of-the-art associated with these challenges and the research gaps, followed by the contributions of this paper.

Many researchers have evaluated day-ahead energy management and optimal power allocation for AC, DC, or AC/DC microgrids including renewable and storage systems through hierarchical multi-level optimization algorithms. In [4], a two-step optimization algorithm is proposed for modified traditional AC distribution networks with

* Corresponding author.
E-mail addresses: salar.moradi@community.unipa.it (S. Moradi), marianogiuseppe.ippolito@unipa.it (M.G. Ippolito), andrea.marletta01@community.unipa.it (A. Marletta), giulia.marcon@unipa.it (G. Marcon), fabio.massaro@unipa.it (F. Massaro), gaetano.zizzo@unipa.it (G. Zizzo).

https://doi.org/10.1016/j.segan.2026.102431
Received 6 March 2026; Received in revised form 2 June 2026; Accepted 17 July 2026
Available online 22 July 2026

Nomenclature

Sets and Indices

Ω_m	Set of microgrid variables.
Ω_b^f	Set of float variables of the b^{th} BESS.
Ω_b^i	Set of binary variables of the b^{th} BESS.
t	Index for time steps.
b	Index for BESS.
s	Index for scenarios.
k	Index for yearly time series unit.
j	Index for time series year.
i	Index for time series day.

Parameters

ω_g	grid power import weighting factor.
N_b	Total number of BESSs.
$P_g^{\max}$	Upper limit for power imported [kW].
C_{PV}/C_{wt}	The capacity of PV and wind turbine systems [kW].
$SoC^{\max}/SoC^{\min}$	Upper and lower limit for SoC.
P_l/P_l^c	Total and critical demand load [kW].
$SoC_b(t=0)$	Initial SoC for b^{th} BESS.
V_{DC}	DC bus voltage [V].
C_b	Capacity of BESS [Ah].
Δt	Time step interval [h].
$\varphi^{dis}/\varphi^{ch}$	Discharge/charge efficiency of BESS' converter [%].
$P_{dis}^{\max}/P_{dis}^{\min}$	Upper and lower bound for discharging power [kW].
$P_b^{\max}$	Maximum power at operation point for BESS [kW].
$P_{ch}^{\max}/P_{ch}^{\min}$	Upper and lower bound for charging power [kW].
μ_{SoC}	off-set SoC to avoid end-of-horizon effect at BESS.
$\Delta SoC^{\max}$	Permissible Range for SoC Variation.
T_f	Fault occurrence time.
T_b	Required time for full charge [h].
E_b	Energy capacity of b^{th} BESS [kWh].
n	Discharge/charge balancing exponent.
$K(0)$	Fixed value for charging/discharging adjustment coefficient.
R_{th}	Charge/discharge weight threshold ratio.
ϵ	Incremental charging adjustment factor.
n_y	Number of available years of observed RESs time series.
n_t	Time series length.
n_B	Number of bootstrap simulations.
δ_t	Daily resampling window's width.

Variables

P_g	Power imported form the main grid [kW].
ω_b	SoC importance weight.
SoC_b	State of Charge of the b^{th} BESS.
K_b	Charging/discharging adjustment coefficient for b^{th} BESS.
P_{pv}/P_{wt}	PV and WT output power [kW].
P_b^{dis}/P_b^{ch}	Discharge/charge power for b^{th} BESS [kW].
i_b^{out}	Output current of b^{th} BESS [A].
I^{dis}/I^{ch}	Discharge/charge binary variables.
P_b^i	Absorbing/injecting power by BESS in islanding mode [kW].
K_{SoC}^i	SoC-based power sharing factor in islanded mode.
T_{out}^i	The time at which the program stop running in islanded mode.
X	Observed RESs time series.
$\widetilde{X}$	Bootstrapped RESs time series.
$\widetilde{\mathbf{X}}_{n_B}$	Matrix with n_B column-vectors bootstrapped RESs time series.
$x_i/\widetilde{x}_i$	Daily data of the observed/bootstrapped RESs time series for the i^{th} day.

dispatchable and renewable generation in smaller regions. It considers the effects of fast and slow EV charging profiles on power supply quality and operating costs. [5] presents a centralized EMS for an on-grid DC microgrid, aiming for maximum PV-storage utilization and minimal power import from the AC grid. The system decides on load shedding based on the storage's SoC. [6] proposes distributed control schemes for solar-storage DC nanogrids in households. A SoC-balancing power flow technique minimizes energy losses across household configurations and communication links. [7] introduces a stochastic optimal load flow approach for AC/DC microgrids to allocate power among DGs and RESs, considering uncertainties in loads, market prices, and RES output. The method employs the Crow Search Algorithm (CSA) to optimize the problem space. Hierarchical power management strategies are discussed in [8] and [9] for AC/DC microgrids. A mixed-integer linear programming (MILP) approach is used at the tertiary level to determine power references for the grid and converter-based DGs. [8] incorporates traditional probability functions, while [9] uses historical data to address RES output, load, and energy price uncertainties. To minimize converter power losses in AC/DC microgrids, some works utilize MILP-based unit commitment strategies. Nonlinear conversion power loss functions, dependent on converter power and DC voltage, are linearized using Neural Network-based models [10] and Linear Surrogate Models [11]. Risk-based energy management is explored in [12–14]. In [12], risk and security constraints are integrated into an energy management framework for on-grid AC/DC networks. Successive MILP solves day-ahead load shifting while conserving voltage through inverters and Volt-VAR control. Uncertainty in loads, energy prices, and RES outputs is addressed with probability density functions and Monte Carlo simulations. [13] uses specific linearization techniques to develop a MILP program for minimizing operational costs and risks due to RES uncertainties in AC/DC energy management systems. Meanwhile, [14] examines grid-connected optimal power sharing among renewables, storage, and EV parking lots, focusing on the resiliency and reliability of off-grid AC/DC microgrids. Few studies emphasize the impact of EV parking lot microgrids on day-ahead optimal power allocation and resilience-oriented scheduling, despite their highly variable charging demand and strong dependence on renewable generation and storage coordination. In [15], technoeconomic optimization indicators are analyzed by comparing Normal, Poisson, and Weibull probability density functions with historical data. [16] develops an algorithm to calculate reserve services from EV charging stations and storage systems, considering PV production uncertainties through chance-based modeling. Almost all the works reviewed above have focused on optimizing power management in on-grid operation mode, without adequately considering the resilience and reliability of power supply during islanded mode when the microgrid transitions to islanding operation due to a fault. Therefore, one of the case studies considered in this paper (MG2) represents an EV parking lot microgrid to evaluate the effectiveness of the proposed framework under EV-related operational variability and seasonal charging demand conditions.

In addition, addressing the uncertainty associated with RESs output power is another challenge in energy management context for AC/DC hybrid microgrids. The references mentioned above have analysed the uncertain variables through stochastic techniques, using well-known probability functions. Since an environmentally data-driven technique is implemented in this paper to consider RESs production intermittent feature, the literature below points the related works. [17] tries to pick a number of representative solar sites using data mining techniques

Table I
Comparison of representative SoC balancing and energy management strategies.

Ref.	Control level	Adaptive charge/discharge	SoC balancing	Islanded resilience	Seasonal scenarios
[27]	Real-time	√	√	x	x
[28]	Real-time	√	√	x	x
[29]	Real-time	√	√	√	x
[30]	Real-time	√	√	x	x
[31]	Real-time	√	√	x	x
This paper	Day-ahead EMS	√	√	√	√

through few months power generation available data to estimate power generation of a large number of solar sites. Several studies have proposed data-driven and learning-based approaches to estimate renewable power generation and uncertainty characteristics using historical environmental and operational data [18–26]. However, most of these methods focus on forecasting architecture and online data processing rather than their integration into day-ahead resilience-oriented energy management and optimal power allocation frameworks for AC/DC microgrids. In these algorithms, current data measured by smart devices must be transported to the main center to be evaluated through an online system that increase the burden and cost of calculations.

Furthermore, to implement proper daily charging/discharging scheduling and SoC balancing strategies for storage systems is vital for distribution operators to achieve reliable long-timescale power allocation, support auxiliary services, and prolong battery lifetime. In the context of day-ahead energy management, the charging/discharging scheduling of BESSs directly influences the feasibility and resilience of optimal power dispatch, especially under varying renewable generation scenarios and islanding events. Previous charging/discharging strategies lie on technical parameters like AC/DC voltages or frequency in AC side, while SoC-based droop controllers are usually adopted for energy balance of BESSs. A SoC-based charging/discharging strategy is implemented in [27], using constant voltage charging strategy and adaptive proportionate charging/discharging to ensure longevity and SoC balancing respectively. [28] proposed a power loss optimization for power dispatch among AC/DC sources including BESSs charging/discharging powers, and an aging rate equalization strategy for SoC balancing. In an autonomous selective prioritized charging/discharging strategy, [29] proposes to shift piecewise P/f characteristics for distributed controlled BESSs to response to SoC balancing and to meet demand. For the control of heterogeneous energy storage systems, [30] proposed an optimal feedback control gain and a weighted control matrix, which guarantee the proportional power sharing and SoC balancing. An improved double-quadrant SoC based droop control strategy is proposed for SoC balance [31] which uses average SoC, and a secondary controller adopts an optimization to achieve power sharing and minimizing voltage deviations. Although these studies provide effective real-time control and power-sharing mechanisms, their primary focus is on short-timescale operational control rather than day-ahead power allocation and scheduling. There are other technical power sharing techniques to prolong BESS lifetime such as flexible power point tracking (FPPT) concept for PV as a primary dc voltage regulator, keeping BESS standby as a secondary regulator through minimizing BESS utilization program [32], in charging current reduction for BESS to prevent overcharging and high SoC [33], and IoT-based droop control [34]. The SoC balancing and BESS power management techniques reviewed above have been analyzed primarily for real-time simulations, not for day-ahead power management. Additionally, variations in PV generation can influence the charging/discharging power rates; however, these studies assume fixed values for these power rates. Furthermore, this paper proposes an autonomous charging/discharging power management approach for BESSs in both on-grid and off-grid modes, allowing them to operate in different modes simultaneously, a feature only considered in [29].

Unlike most existing studies, which mainly focus on converter-level real-time control or droop-based SoC balancing, the proposed framework integrates adaptive SoC-dependent charging/discharging scheduling into a day-ahead MILP-based optimal power allocation problem for AC/DC microgrids. Therefore, the main research gap lies in integrating seasonal renewable uncertainty analysis, long-timescale SoC-aware power allocation, and resilience-oriented islanded operation assessment into a unified day-ahead EMS framework for AC/DC microgrids. Table I provides a comparative summary between the proposed framework and representative existing methods, highlighting the distinct features of the proposed day-ahead resilience-oriented EMS strategy for AC/DC microgrids.

Building on the reviewed literature and identified research gaps, this paper proposes a simple yet effective framework to address these gaps in day-ahead energy management for AC/DC microgrids. The main contributions of this work can be summarized as follows:

- A SoC balancing strategy is implemented in both grid-connected and islanded operating modes for microgrids with multiple BESSs, aiming to prevent overcharging and deep discharging. The proposed adaptive SoC-based charging/discharging scheduling framework is integrated into the day-ahead optimal power dispatch problem, enabling efficient long-timescale energy allocation among BESS units while improving operational resilience during islanded operation. The SoC-based charging/discharging power management and the proposed SoC balancing strategy make the algorithm autonomous, allowing BESSs to operate in different modes simultaneously.
- Renewable energy forecasts within the energy management system are modeled through a data-driven approach based on bootstrap resampling for dependent data. This method generates synthetic time series of renewable energy sources while preserving seasonal patterns and statistical variability, ensuring more realistic inputs for the day-ahead power allocation framework and scenario analysis.
- Seasonal variations in load demand and renewable power generation can lead to changes in the power curtailment of RESs, potentially causing infeasibility in the optimization program as BESSs may reach their maximum allowable SoC. To address this, the charging/discharging power rates of BESSs must be reduced to achieve feasible solutions across all seasons. Accordingly, the paper investigates the influence of BESS charging/discharging rate limits on the feasibility and effectiveness of long-timescale optimal dispatch under different seasonal energy scenarios.

This paper is organized as follows: Section II models the energy management framework for both on-grid and offgrid operating modes. Section III describes the generation of environmental-based energy scenarios for RES output power. Section IV discusses and formulates the adaptive SoC logic integrated into the objective function to implement efficient charging/discharging modes, SoC balancing strategies, and battery parameter tuning. Sections V and VI represent the case studies description and scenario generation respectively. Simulation results are discussed in section VII. Finally, section VIII concludes the paper.

2. Energy management programming

In this section energy management program for a general AC/DC microgrid in both grid-connected and islanded modes is formulized. Now, for any network, assuming we have all the required initial data for load, BESSs, and RESs, we can proceed. It is assumed that the load changes monthly or seasonally, depending on the data stored, throughout the year, while historical data for environmental variables, such as wind speed, solar irradiation, and temperature, is available for each 15-minute interval over the year. The following subsections analysis both grid-connected and islanding operation modes.

2.1. Grid-connected operation mode

For each day, divided into 96 time steps of 15-minute, the optimization program is modeled. In grid-connected mode, the objective function is to minimize power imported from the main grid (P_g) while maximizing SoC in the BESSs. This is because, in this paper, security and reliability factors are more important than economic ones. The aim is to ensure that the SoC in the batteries is high enough to supply critical loads or even higher in the event of a fault, when the network is disconnected from the main grid for some time intervals though. In this way, the cost of purchasing power is minimized, while ensuring sufficient energy is stored in the BESSs. Although in this paper, reliability indices measurements and storage utilization in islanded mode, are analysed for a day ahead time interval after fault, sufficient SoC refers to being able to supply critical load along with RESs' power for less than one hour as fault clearness is assumed takes 45 min here.

Since the programming is implemented in Python, the objective function, along with all equality and inequality constraints, needs to be organized as sets. To achieve this, the variable vector is first introduced to clarify the order of variables. This ensures that, for the equations presented in this paper, readers can easily understand the cell in which the coefficients of each variable must be placed in the corresponding set. The note is that this program is developed for a general AC/DC hybrid microgrid with total number of BESS N_b. Thus, the microgrid variable set is:

$$\Omega_m = \left\{P_g, \Omega_1^f, \Omega_2^f, \ldots, \Omega_{N_b}^f, \Omega_1^i, \Omega_2^i, \ldots, \Omega_{N_b}^i\right\} \tag{1}$$

Where $\Omega_b^f = \{P_b^{dis}, P_b^{ch}, SoC_b\}$ and $\Omega_b^i = \{I^{dis}, I^{ch}\}$ are the sets of float and binary variables for each BESS respectively. The program asks the user to choose a day in a month of a season. So, objective function for each time step and each scenario is as follows.

$$\text{O.F.} = \min\left[\omega_g P_g(t) + \sum_{b=1}^{N_b} \omega_b(t) \cdot SoC_b(t)\right] \quad \forall t, s \tag{2}$$

Since the dimension of P_g is in kW and SoC is a percentage of the BESS capacity, they need to be normalized by their corresponding weights to make them comparable. ω_g depends on the network's limit for importing power from the main grid, as follows:

$$\omega_g = \frac{1}{P_g^{\max}} \tag{3}$$

The weight of SoC depends on the strategy for charging/discharging cycles of the BESSs. The proposed strategy in this paper makes the battery with a high SoC operate in discharging mode, while the battery with a low SoC begins to charge. Therefore, ω_b for each BESS is a dynamic function of the corresponding SoC at each time step. A lower SoC increases the importance coefficient of the SoC variable, causing the battery to begin charging, while a higher SoC inversely reduces the importance of the SoC, prompting the battery to start discharging. So, ω_b is calculated as:

$$\omega_b(t) = K_b(t)\frac{SoC^{\max}}{SoC_b(t)} \quad \forall b, t \tag{4}$$

Where, K_b is charging/discharging adjustment coefficient for b^{th} BESS. From Eq. (4), it is clear that depends on two dynamic variables, SoC and K_b. When the SoC reaches low values, for example 0.25, Ω_b increases enough to initiate charging. In this case, if K_b had increased, the BESS would start charging earlier, at SoC $= 0.5$, for example. Therefore, K_b determines the threshold between charging and discharging modes.

Additionally, regarding the charging/discharging strategy in this paper, it is desirable for the BESS to have a few full charging/discharging cycles per day. This is because small oscillations in the SoC reduce the battery's lifetime. If the SoC starts rising after a full discharge cycle but then discharges again in the next time step, oscillations between these two operation modes become observable. To avoid this, a dynamic K_b is presented in this paper, which is updated at each iteration precisely when the operation mode switches to charging to ensure continuity. K_b is updated as follows:

$$K_b(t) = K_b(t-1) + \varepsilon \quad \forall b, t \tag{5}$$

A higher ϵ damps the number of swings, resulting in a faster charging mode. The initial ω_b, or $\omega_b(t = 0)$, is calculated based on the initial SoC and K_b, specifically $SoC(t = 0)$ and K_b $(t = 0)$, respectively. The tuning of the initial values for K_b and ϵ is described in detail in section IV.

Now, operational and technical constraints need to be considered in the optimization. These constraints are divided into two groups: equality and inequality constraints. The first equality constraint represents the power balance between generation and load consumption at each time step, expressed as follows:

$$P_g(t) + P_{pv}(t) + P_{wt}(t) + \sum_{b=1}^{N_b} P_b^{dis}(t) = P_l(t) + \sum_{b=1}^{N_b} P_b^{ch}(t) \quad \forall t, b \tag{6}$$

The next equality constraint is used to calculate the SoC for each BESS based on the charging/discharging power. Before doing this, it is important to first determine the relationship between the SoC of the BESS and its power output. The common coulomb counting method is used in this paper to determine the SoC of each BESS unit at each time step, as shown below:

$$SoC_b(t) = SoC_b(t-1) - \frac{1}{C_b}\int i_b^{out}(t)dt \quad \forall t, b \tag{7}$$

Where $i_b^{out}(t)$ represents the output current of the battery, which is calculated as:

$$i_b^{out}(t) = P_b^{out}(t).V_b^{out}(t) \quad \forall t, b \tag{8}$$

Where $P_b^{out}(t)$ and $V_b^{out}(t)$ represent the output power and voltage of the battery, respectively. In Eq. (8), $P_b^{out}(t)$ is positive when the battery is in discharge mode, causing the SoC to decrease, while the charging power is negative, resulting in an increase in SoC. Additionally, $V_b^{out}(t) \approx V_{DC}$, where the DC-link voltage is assumed to be tightly regulated by the power electronic converters and remains nearly constant over a wide range of SoC values in the day-ahead energy management model. Authors acknowledge that in detailed converter-level droop control strategies, voltage deviations can indeed be used to induce circulating power flows between storage units [35]. However, such fast-timescale control dynamics are outside the scope of this day-ahead MILP energy management formulation. Thus, by combining Eqs. (7) and (8), the following expression is derived:

$$SoC_b(t) = SoC_b(t-1) - \frac{1}{V_{DC}\,C_b}\int P_b^{out}(t)dt \quad \forall t, b \tag{9}$$

Since this paper assumes a linear optimization program with fixed 15-minute time steps, Eq. (9) can be rewritten as:

$$SoC_b(t) = SoC_b(t-1) - \frac{P_b^{dis}(t)\Delta t\, \varphi^{dis}}{V_{DC}\,C_b} + \frac{P_b^{ch}(t)\Delta t}{V_{DC}\,C_b\,\varphi^{ch}} \quad \forall t, b \tag{10}$$

In equations above, $SoC_b(t)$, $P_b^{dis}(t)$, and $P_b^{ch}(t)$ are variable and other parameters are fixed and defined as: $\Delta t = 0.25$ h (that is 15 min per hour), φ^{dis} and φ^{ch} are discharging and charging efficiency for converters connected to batteries that is between 0.9 and 1, V_{DC} is DC bus voltage, and C_b is the battery capacity in ampere-hour, calculated as $C_b = \frac{E_b}{V_{DC}}$, where E_b is the energy capacity of BESS unit in kWh. In this work, some inequality constraints are established. The first constraint states that charging and discharging cannot occur simultaneously, and that these powers should be less than their maximum and greater than their minimum rates. To implement this, binary variables are used so that if the program chooses to operate the BESS in discharge mode, the corresponding binary variable I_b^{dis} would be 1 and I_b^{ch} would be 0; conversely, for charge operation mode, $I_b^{dis} = 0$ and $I_b^{ch} = 1$. These limits are formulated in Eqs. (11)-(13) as follows:

$$I_b^{dis}(t)\cdot P_{dis}^{\min} \leq P_b^{dis}(t) \leq I_b^{dis}(t)\cdot P_{dis}^{\max} \quad \forall t, b \tag{11}$$

$$I_b^{ch}(t)\cdot P_{ch}^{\min} \leq P_b^{ch}(t) \leq I_b^{ch}(t)\cdot P_{ch}^{\max} \quad \forall t, b \tag{12}$$

$$I_b^{dis}(t) + I_b^{ch}(t) \leq 1 \quad \forall t, b \tag{13}$$

There are additional technical limitations for BESS units, derived in Eqs. (14)–(17). Inequality (14) prevents the energy level at the last hour of BESS operation from being significantly higher or lower than that of the first hour, where μ_{SoC} is set to 0.4 in this paper. Additionally, based on the calculated maximum charging/discharging power, the SoC at each time step cannot change by more than the maximum allowed value, as derived in Eq. (15). Section IV explains how to calculate the maximum charging and discharging powers, as well as $\Delta SoC^{\max}$. Eq. (16) ensures that the SoC remains within its upper and lower limits. The equality presented in (17) is a technical consideration, as one of the primary aims of this work is to ensure the supply of critical loads when the microgrid is disconnected from the main grid due to a fault. It is assumed that each fault lasts an average of 45 min; therefore, the energy stored in all BESS units must be sufficient to supply the critical load for three time steps, as described in (17). Note that in Eq. (17), the second term defines the critical load power as the energy required to supply the critical load.

$$|SoC_b(t = 96) - SoC_b(t = 0)| \leq \mu_{SoC} \quad \forall b \tag{14}$$

$$|SoC_b(t) - SoC_b(t-1)| \leq \Delta SoC^{\max} \quad \forall b, t \tag{15}$$

$$SoC^{\min} \leq SoC_b(t) \leq SoC^{\max} \quad \forall b, t \tag{16}$$

$$\sum_{b=1}^{N_b} SoC_b(t) = N_b\cdot SoC^{\min} + \sum_{t=T_f}^{T_f+2} \frac{P_l^c \Delta t\, \varphi^{dis}}{V_{DC}\, C_b} \quad \forall b, t \tag{17}$$

Where, $SoC^{\min}$ and $SoC^{\max}$ are 0.2 and 0.9, respectively. Additional technical constraints depend on the BESS operation modes (charge/discharge), as explained in Section IV. Finally, the power imported from the main grid must remain below its upper limit, as follows:

$$0 \leq P_g(t) \leq P_g^{\max} \quad \forall t \tag{18}$$

2.2. Islanded operation mode

In islanded operating mode, the SoC strategy is straightforward. Depending on the difference between the power output of renewable sources and the critical load demand, storage units can either inject or absorb power. This difference for a general power grid can be expressed as:

$$P_b^i = P_{pv} + P_{wt} - P_l^c \tag{19}$$

When $P_b^i > 0$, it indicates that renewable sources can supply the load demand, and the excess power can be absorbed by the storage units, causing the BESSs to operate in charging mode, where $P_b^{ch} = P_b^i$. Conversely, when $P_b^i < 0$, storage units need to inject power into the microgrid to compensate for the power generation shortage, making the BESSs operate in discharging mode where $P_b^{dis} = P_b^i$. Regardless of whether the storage units operate in grid-connected or islanded mode, a SoC balancing strategy is implemented to prolong the lifetime of the BESSs. These strategies for each operating mode are discussed in Section IV.

It is worth mentioning that, although a simplified MILP approach is applied in the proposed method and does not fully capture nonlinear behaviors such as battery degradation costs and converter performance characteristics, it still supports the intended objectives without loss of generality for day-ahead energy management applications. Neglecting detailed battery aging costs may introduce economic deviations in long-term operational studies, particularly under frequent deep charging/discharging cycles. However, the proposed adaptive SoC-based charging/discharging scheduling and SoC balancing strategies inherently mitigate excessive cycling and overutilization of BESSs, thereby partially reducing degradation-related impacts during operation. In addition, simplified converter efficiency assumptions are adopted to preserve the linear structure and computational tractability of the MILP optimization problem. Since converter efficiencies generally operate within limited practical ranges during normal operation, the resulting deviations in power loss estimation are expected to remain limited for day-ahead dispatch studies. The study primarily aims to evaluate the impact of external conditions and operational characteristics, such as the SoC of BESSs, on the load supply reliability and resilience of AC/DC microgrids under different operating scenarios. Therefore, the adopted simplifications are considered appropriate for operational scheduling and resilience-oriented analysis, while more detailed nonlinear battery and converter models may be incorporated in future work for high-fidelity technoeconomic assessments.

3. Environmental-based energy scenarios generation

This section introduces a methodology for simulating realistic renewable energy sources for scenario analysis. RESs are modeled as univariate time series, where a modified version of the block bootstrap resampling method is implemented to generate realistic time series over a one-year period. The objective is to produce an arbitrary number n_B of synthetic annual series for key RESs, such as wind speed, solar irradiation and temperature. This method validates that the generated series maintain the same statistical properties of the original data by exhibiting the same temporal dependencies, seasonality and autocorrelation structure. This ensures that the generated synthetic series realistically reflect the behavior of the observed data and enable the assessment of the variability and uncertainty of RESs, making them a reliable tool for scenario analysis. Similar resampling approaches have been applied in [36] and [37].

Adequately long time series and stationary trends are required in order to apply such methodology. Let $X = \{X_1, \ldots, X_j, \ldots, X_{n_y}\}$ represent the observed historical time series, where each yearly time series is defined with respects to the available time unit:

$$X_j = \{x_{j,1}, \ldots, x_{j,k}, \ldots, x_{j,n_t}\} \tag{20}$$

where $j = 1, \ldots, n_y$ denotes the variable number of years, and $k = 1, \ldots, n_t$ represents the times series frequency.

The resampling procedure is applied at daily level; thus, observations are grouped into 24-hours blocks. The entire yearly bootstrapped $\widetilde{X} = \{\widetilde{x}_1, \ldots, \widetilde{x}_i, \ldots \widetilde{x}_{365}\}$ time series is generated by resampling each day $\widetilde{x}_i$ from a bounded and symmetric neighborhood of the same i-th day of all the n_y years. The goodness of the resampling procedure is related to the neighborhood width δ_t around each day. To preserve annual seasonality, the proposal consists of daily resampling which are performed locally by using a moving resampling window of width δ_t (positive integer).

The whole bootstrap process consists of repeating the above pro-

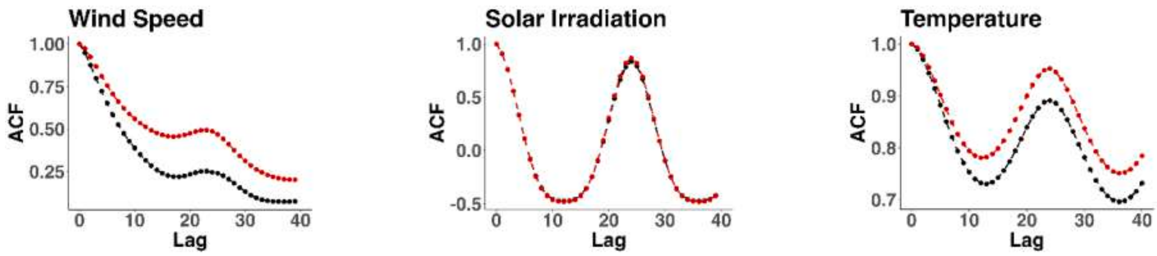

Fig. 1. Autocorrelation function (ACF) for the observed (red line) and simulated (black line) wind speed, solar irradiation and temperature data.

cedure n_B times in order to obtain the matrix $\widetilde{\boldsymbol{X}}_{n_B} = [\widetilde{X}_1, \ldots, \widetilde{X}_{n_B}]$, where each column vector is a resampled time yearly time series.

Algorithm 0. describes the resampling moving-window block bootstrap procedure in details. Notice that the annual series $\widetilde{X}_j$ is treated as circular. Thus, in line eight of the algorithm 0, when $i - \delta_t < 0$ or $i + \delta_t > 365$ (where the interval will not contain all $2\delta_t + 1$ possible elements), the interval extends into the end of the previous year or into the beginning of the next year, respectively.

To assess the reliability of the generated time series, their statistical properties are compared with those of the input data. In an explanatory analysis, $n_B = 100$ synthetic annual series are

Algorithm 0. : Resampling Moving-Window Block Bootstrap.

1 Import X (observed time series)
2 Set the empty matrix $\widetilde{\boldsymbol{X}}_{n_B}$ with n_B columns
3 Set the resampling window width δ_t
4 *for* $h \in$ range(n_B)
5   Set the empty vector $\widetilde{X}_h$
6   *for* $i \in$ range(365)
7   Randomly sample the index of one year $j = 1, \ldots, n_y$
8   Randomly sample one day $\tilde{x}_i$ of the year j from the interval $[x_{i-\delta_t}, x_{i+\delta_t}]$
9   Let $\widetilde{X}_h[i] = \tilde{x}_i$
10   *end*
11   Let $\widetilde{\boldsymbol{X}}_{n_B}[, h] = \widetilde{X}_h$
12 *end*
13 Return $\widetilde{\boldsymbol{X}}_{n_B}$

generated for wind speed, solar irradiation, and temperature, using a resampling window with width $\delta_t = 10$. Results show good performances of the resampling methodology. Fig. 1 compares the autocorrelation functions (ACF) of the observed and simulated series (red and black lines, respectively). The first panel (wind speed) shows that while the simulated ACF follows the original trend for small lags, deviations occur for higher lags. This suggests that the bootstrapped series capture short-term dependencies but may only approximate long-range correlations. However, the sinusoidal damping pattern in the ACF correctly reflects the day-night cycle. The second panel (solar irradiation) shows that the simulated series effectively reproduce the observed ACF, maintaining the periodicity and seasonal structure. The third panel (temperature) shows a slightly underestimation of the original ACF after lag 10.

Fig. 2 presents seasonal mean profiles for the 100 simulated series (gray lines) and the original dataset (red line). The bootstrapped series closely follow the seasonal trends of the observed data, with expected variability around the historical mean.

The approach described provides a practical way to generate realistic time series while preserving key statistical properties, local temporal structures and seasonal variations without imposing strong model assumptions. Although some long-range dependencies may not be fully preserved, and extreme events beyond the historical dataset cannot be generated, the method is not computationally demanding. The generated series reflect the observed variability while allowing for the creation of multiple plausible realizations and remains a useful tool for scenario-based simulations where statistical consistency is required.

Next, five environmental-based energy scenarios are considered, defined on the basis of the empirical distributions of RESs:

- Baseline scenario
- Reduced wind speed
- Increased wind speed
- Reduced solar irradiance
- Increased temperature

The *Baseline scenario* is generated by computing the hourly mean, across the n_B bootstrapped realizations, for a selected day. *Reduced wind speed* scenario derives from the following procedure: given a selected day of the year, compute the 24-hours wind speed average over the n_B generated data; this provides the related empirical distribution where the day which corresponds to the 5^{th} percentile is selected. In the same scenario, solar irradiance and temperature values corresponds to the baseline scenario in order to isolate the effect of wind speed reduction

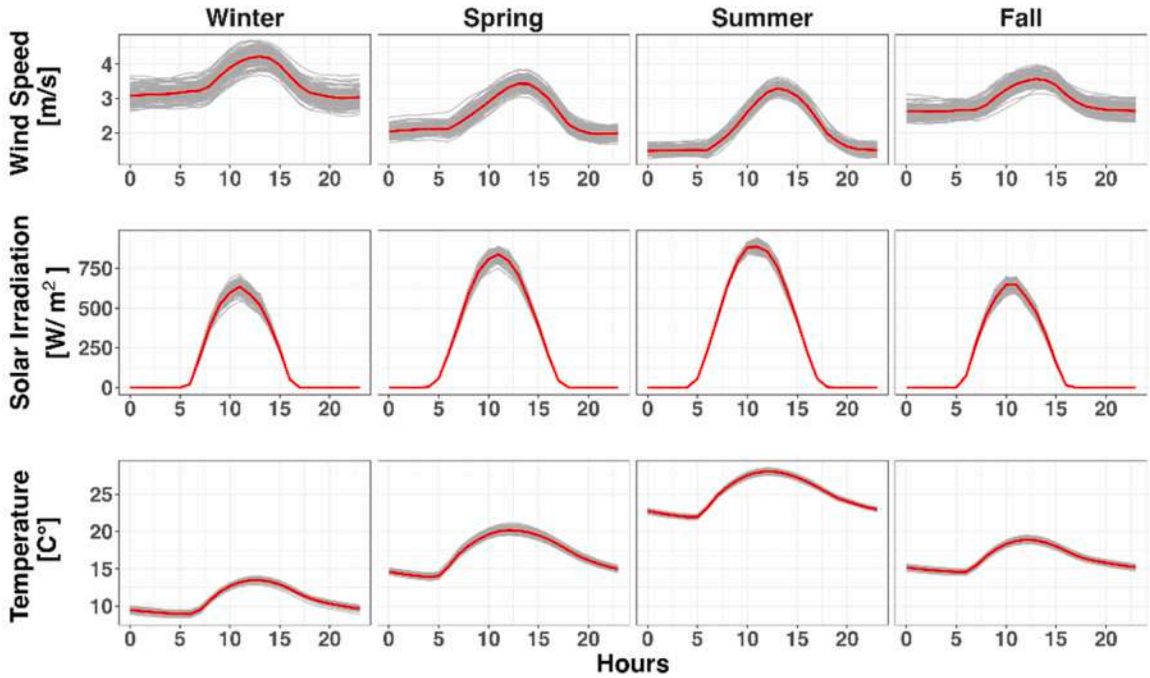

Fig. 2. Seasonal profiles, from left to right the seasonal progression, from top to bottom: wind speed, solar irradiation and temperature. Simulated series in gray, original series in red.

from other influencing factors. The approach which generates the *Increased wind speed* scenario refers to the same empirical distribution on 24-hours wind speed averages whereas the selected day coincides with the 95th percentile keeping solar irradiance and temperature values as in the baseline scenario. Similarly, the *Reduced solar irradiance* and *Increased temperature* scenarios are generated by applying the same percentile-based selection criterion to their respective variables while keeping the others at baseline conditions.

4. BESS operation and SoC balancing strategies

This section explains how BESS charging and discharging cycles, as well as SoC balancing strategies, are managed in the proposed linear programming model for both grid-connected and islanded operating modes. Before analyzing these strategies, some basic calculations for the batteries used in the previous formulations are outlined here. Assuming a battery unit with capacity $C_b = \frac{E_b}{V_{DC}}$, where E_b is the energy capacity of BESS unit in kWh, and assuming a full charge time of 4 h ($T_b = 4$), the maximum output current for the b^{th} battery is calculated as:

$$i_b^{\max} = \frac{C_b}{T_b} \tag{21}$$

Thus, the maximum injected power (in both discharge and charge modes) is calculated as:

$$P_{ch}^{\max} = P_{dis}^{\max} = I_b^{\max} \cdot V_{DC} \tag{22}$$

As a result, maximum allowed change in SoC can be calculated as follows:

$$\Delta SoC^{\max} = \frac{P_{dis}^{\max} \Delta t}{V_{DC}\, C_b} \tag{23}$$

4.1. Grid-connected operation mode

In grid-connected mode, charge or discharge operating modes for the BESS are established based on the SoC of the batteries in the proposed model. In this strategy, as described in Eq. (4), when the SoC is close to its upper limit, the battery begins to discharge since the corresponding weight is significantly lower than that of the power imported from the main grid. Coefficient K_b tuning is also based on this principle, as it is preferable for the battery to continue discharging fully to extend its lifetime by reducing cycling, while still respecting the critical load supply constraint in Eq. (17). Furthermore, to prolong the lifespan of the BESS units and prevent overuse of any single BESS, each storage unit's SoC should be balanced, and the injected/observed output power should be gradually equalized. For instance, if two storage units, b1 and b2, are both in discharge mode and $SoC_{b1}(t) > SoC_{b2}(t)$, the first unit should inject more power than the second to allow their SoC levels to converge over time. This strategy might be implemented as a constraint in the optimization program as follows:

$$P_{b1}^{dis}(t) > P_{b2}^{dis}(t) \left(\frac{SoC_{b1}(t-1)}{SoC_{b2}(t-1)} \right)^n \quad \forall t \tag{24}$$

Eq. (24) ensures that the BESS unit with a higher SoC injects more power than the other unit. The balancing exponent n determines the rate at which the SoC values converge. The value of n depends on the SoC difference and the operators' preference for convergence speed. Experimentally, a range of $3 \le n \le 8$ is typical, with $n = 5$ being a reasonable choice for the strategy proposed in this paper.

Conversely, when the SoC of storage units reaches a lower value, the unit with the lower SoC must absorb more charging power to increase quickly SoC and converge with the units with higher SoC. In an example with two units, where $SoC_{b1}(t) > SoC_{b2}(t)$, the charging power is formulated as follows:

$$P_{b2}^{ch}(t) > P_{b1}^{ch}(t) \left(\frac{SoC_{b1}(t-1)}{SoC_{b2}(t-1)} \right)^n \quad \forall t \tag{25}$$

In general, in a network with N_b storage units, where $\max\{SoC_{b1}, \ldots, SoC_{N_b}\}$ represents the BESS with the highest SoC; therefore, this SoC is used as the nominator in the exponent part of (24) and (25). An important aspect of this strategy is that once storage units begin charging, they should continue charging until fully charged to avoid frequent switching between charging and discharging modes, which reduces their lifetime. Therefore, the proposed adaptive charging/discharging scheduling strategy indirectly supports battery lifetime preservation by reducing unnecessary mode switching and preventing prolonged operation near extreme SoC limits. According to Eq. (4), when the SoC is sufficiently low, the program selects the charging mode. As the SoC increases slightly, however, ω_b drops, potentially prompting a return to discharge mode. To prevent this, a dynamic coefficient K_b is introduced and updated in each iteration to increase ω_b (Eq. (5)), thus maintaining the charging mode. The formulation for this adjustment coefficient is given as follows:

$$K_b(t) = \begin{cases} K(0) & \text{if } SoC_b(t) < SoC_b(t-1) \\ \text{Eq.}(5) & \text{if } SoC_b(t) \geq SoC_b(t-1) \end{cases} \quad \forall t, b \tag{26}$$

In (26), when $SoC_b(t) < SoC_b(t-1)$, storage unit is in discharge mode, so K_b does not change and remains at the initial value $K(0)$. Anyway, when $SoC_b(t) \geq SoC_b(t-1)$, storage unit has already switched to charge mode; therefore, K_b needs to be updated by adding charging incremental adjustment factor ϵ to hold charging mode. Higher ϵ leads to decrease in charging/discharging swing and in the speed of SoC rise. The next section explains how to tune $K(0)$ and ϵ. In the proposed framework, the adaptive charging/discharging logic is updated only after obtaining a feasible solution from the MILP optimization program at each time step. According to the optimization program discussed in Section II, and the BESS charging/discharging strategy in this subsection, the general proposed algorithm is described in Algorithm 1.

4.2. Islanded operation mode

Based on the power management and dispatch between RESs and storage systems discussed in the subsection B of the section II, P_b^i can either be injected into or absorbed by the BESS. For microgrids with two or higher BESSs, this power needs to be shared among all units based on their current SoC exactly before the fault time (T_f) to achieve SoC balancing. This strategy is similar to the one implemented in grid-connected mode, except that it does not account for the effect of the BESS charging/discharging adjustment coefficient K_b. To achieve SoC balancing, for example in a microgrid with two BESSs, lets first define a SoC-based power sharing factor k_{soc}^i as:

$$k_{soc}^i = \left(\frac{SoC_{b1}(t = T_f)}{SoC_{b2}(t = T_f)} \right)^n \tag{27}$$

This factor initiates the SoC balancing program in islanded mode. The SoC of the BESSs for the next time step can then be calculated as follows for the charging mode ($P_b^i > 0$).

$$\begin{cases} SoC_{b1}(T_f + 1) = SoC_{b1}(t = T_f) + \dfrac{P_b^i \Delta t \varphi^{ch}}{V_{DC} C_b \left(1 + k_{soc}^i\right)} \\ SoC_{b2}(T_f + 1) = SoC_{b2}(t = T_f) + \dfrac{P_b^i \Delta t k_{soc}^i \varphi^{ch}}{V_{DC} C_b \left(1 + k_{soc}^i\right)} \end{cases} \tag{28}$$

And for discharging mode ($P_b^i < 0$),

$$\begin{cases} SoC_{b1}(T_f + 1) = SoC_{b1}(t = T_f) - \dfrac{P_b^i \Delta t k_{soc}^i}{V_{DC} C_b \left(1 + k_{soc}^i\right) \varphi^{dis}} \\ SoC_{b2}(T_f + 1) = SoC_{b2}(t = T_f) - \dfrac{P_b^i \Delta t}{V_{DC} C_b \left(1 + k_{soc}^i\right) \varphi^{dis}} \end{cases} \tag{29}$$

In charging mode, when $SoC_{b1} > SoC_{b2}$, Eq. (28) ensures that the second battery absorbs more power since $k_{soc}^i > 1$, while the first battery injects more power into the grid in discharging mode according to (29). The same analysis applies when $SoC_{b1} < SoC_{b2}$. The note

Algorithm 1. : Optimization program in grid-connected mode

Ask the user to choose the microgrid configuration, loads, microgrid, and main grid characteristics $\leftarrow P_l, P_l^c, P_g^{max}, V_{DC}$
Import the number of BESSs and their characteristics $\leftarrow N_b, SoC^{max}, SoC^{min}, SoC_b(t=0), E_b, T_b$, Eq. (21)–(23)
Import solar irradiation, wind speed, and temperature to produce various scenarios of RES power output $\leftarrow P_{pv}(s), P_{wt}(s)$ in Section III
Initialize charging/discharging and SoC balancing parameters $\leftarrow K_b = K(0) = 0.5, \epsilon = 0.4, n = 5$
Initialize the weights ω_g and $\omega_b(t=0) \leftarrow$ Eq. (3) and Eq. (4)
for $i \in$ scenario set
  for $t \in$ range(96)
    Create objective function vector $\leftarrow \Omega_m$ and Eq. (2)
    Define equality constraints $\leftarrow$ Eq. (6), Eq. (10), and Eq. (17)
    Define inequality constraints $\leftarrow$ Eq. (11)–(16) and Eq. (18)
    if $t > 1$
      SoC balancing strategy is conducted $\leftarrow$ Eq. (24) and Eq. (25)
    end
    Call MILP solver to solve the optimization
    Verify feasibility and extract optimization results
    if $SoC(t) - SoC(t-1) \geq 0 \leftarrow$ charging mode
      Update $K_b \leftarrow K_b + \epsilon$
    end
    if $SoC(t) = SoC^{max} \leftarrow$ discharging mode
      Update $K_b \leftarrow K(0)$
    end
  end
end
Return results

is that, after fault occurs and the microgrids start operating in islanded mode, the proposed analysis is implemented for the next day ahead, meaning from T_f to $T_f + 96$.

In the proposed islanded-mode analysis, the charging and discharging efficiencies are assumed approximately identical for all BESS units. Therefore, the SoC balancing strategy mainly depends on the SoC-based sharing factor k^i_{soc}, which determines the long-timescale power allocation among storage systems according to their available energy levels. This assumption is considered acceptable for the intended day-ahead resilience and operational scheduling analysis. However, in practical implementations, heterogeneous converter efficiencies and battery characteristics may influence the exact power-sharing dynamics.

In addition, the procedure above is continued till RESs and BESSs can supply the critical load, so when BESSs operate in discharging mode ($P^i_b < 0$) and their current SoC has reached to the lower limit 0.2, the program is ended, and the final results are extracted. This is significant because reliability analysis can be conducted for the different scenarios discussed in Section III. The objective is to identify which scenarios represent the best and worst cases from a reliability perspective. Unlike classical reliability indices such as Loss of Load Probability (LOLP), Expected Energy Not Supplied (EENS), and System Average Interruption Duration Index (SAIDI), which typically require probabilistic component reliability parameters such as failure rates and repair times, the proposed indices focus on the operational resilience and supply capability of RESs and BESSs during islanded operation under different energy scenarios. Assuming T^i_{out} represents the time step at which the program stop running, the first index is defined as Renewable and Storage Availability Duration Index (RSADI), and is expressed as:

$$\mathrm{RSADI} = \frac{1}{4}\sum_{Jan}^{Dec}\sum_{T_f=1}^{96}\frac{T^i_{\mathrm{out}} - T_f}{96} \tag{30}$$

This normalized index varies between 0 and 1, where higher values indicate a longer duration during which renewable and storage resources can continuously supply the critical load during islanded operation. In this work, the reported values represent average daily resilience performance evaluated over different annual and seasonal scenarios.

This index represents the percentage of the day during which the generation can supply the critical load. The second index, referred to as the Renewable and Storage Load Supply Index (RSLSI), indicates the percentage of load supply frequency and is defined as:

$$\mathrm{RSLSI} = \frac{1}{4}\sum_{Jan}^{Dec}\sum_{T_f=1}^{96}\frac{\sum_{t=T_f}^{T^i_{out}} P^c_l(t)}{\sum_{t=T_f}^{T_f+96} P^c_l(t)} \tag{31}$$

Similarly, RSLSI is a normalized index ranging between 0 and 1, where larger values indicate a higher frequency of successful critical load supply throughout the studied daily operating horizon. Therefore, RSADI and RSLSI provide complementary resilience-oriented operational information for scenario-based islanded microgrid analysis.

Algorithm 2 represents the power and SoC management for a microgrid operating in islanded mode.

Algorithm 2. : Power and SoC management in islanded mode

Call SoC vectors from Algorithm 1
for T_f in range(1,96)
    for $i \in$ scenario set
        Initialize P_{pv}, P_{wt}, and $SoC = SoC(0{:}T_f)$
        Calculate $k_{soc_i} \leftarrow$ Eq. (27)
        for $t \in$ range(T_f, $T_f + 96$)
            Calculate $P_{b_i} \leftarrow$ Eq. (19)
            if $P_{b_i} \geq 0$
                Charging mode
                Calculate $SoC(t) \leftarrow$ Eq. (28)
                else
                Discharging mode
                Calculate $SoC(t) \leftarrow$ Eq. (29)
            end
            if $SoC(t) = SoC^{min}$
                break
            Update $k_{soc_i} \leftarrow$ Eq. (27)
        end
        Calculate reliability indices RSADI, RSLSI ← Eq. (30) and Eq. (31)
    end
end
Return results

4.3. Parameters tuning for SoC management

In the previous section, the strategy for SoC management of BESS units was described. As noted, when the SoC is high, the program encourages the storage units to inject discharge power into the microgrid, while they switch to charging mode to absorb power if the SoC is low. To implement this strategy, according to Eqs. (2) to (5) in Section II, a weight factor ω_b in terms of a dynamic parameter K_b and the SoC of the storage units is proposed. As outlined in Section IV, K_b is the charging/discharging adjustment coefficient, which remains fixed during discharge mode but is variable during charge mode. This section explains how the fixed value for K_b is determined and how it can be adjusted when the storage unit is in charging mode. Let's begin with the

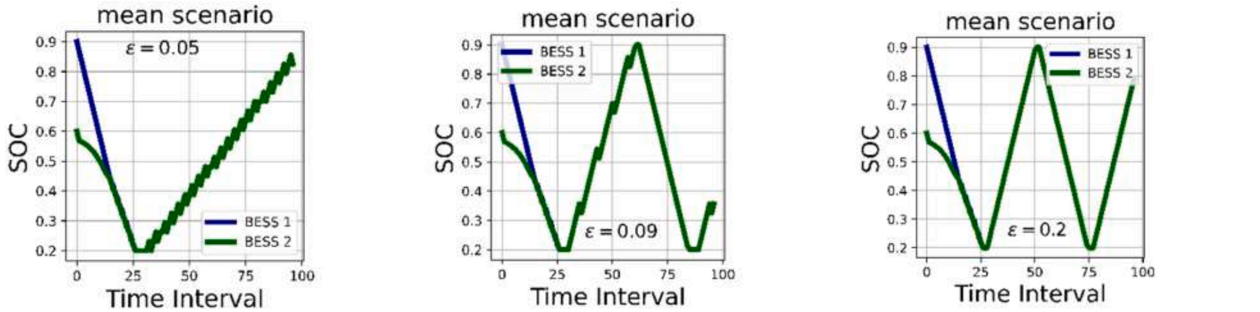

Fig. 3. The impact of ϵ on SoC charging strategy.

discharge mode to calculate $K(0)$ when the BESS is in discharge mode. Before this, a charge/discharge weight threshold ratio R_{th} is defined to ensure that the BESS operates in discharge mode if $\frac{\omega_b}{\omega_g}$ is lower than this threshold, and in charging mode otherwise. Therefore, to remain in discharge mode, the following inequality (32) must be satisfied.

$$\frac{\omega_b}{\omega_g} \le R_{th} \quad \forall b \tag{32}$$

Note that R_{th} is determined experimentally and varies from network to network, as ω_g depends on $P_g^{\max}$. For instance, in a case study with one BESS where $P_g^{\max} = 1500$ kW, $R_{th} \approx 2000$. Moreover, when $SoC_b(t) = SoC^{\max}$, the ratio of the SoC weight to the P_g weight $\frac{\omega_b}{\omega_g}$ must be less than R_{th} to ensure that BESS operates in discharge mode. Therefore, according to (4), the upper limit for K_b can be calculated as:

$$\frac{K(0)}{\omega_g} < R_{th} \quad \forall b \tag{33}$$

In the example mentioned above, if $1500K(0) \le 2000$, then $K(0) \le 1.33$. According to the charging strategy, storage units must start to operate in charge mode when $SoC_b(t) = SoC^{\min}$. The same logic is applied to the charge mode, where $\frac{\omega_b}{\omega_g}$ must be greater than R_{th} to ensure that BESS operates in charge mode. Therefore, using (4) and substituting $SoC_b(t) = SoC^{\min}$, the lower bound for K_b can be derived as follows:

$$\frac{K(0)SoC^{\max}}{\omega_g\, SoC^{\min}} \ge R_{th} \tag{34}$$

In the example above, with $SoC^{\max} = 0.9$ and $SoC^{\min} = 0.2$, it is derived that $K(0) \ge 0.3$.

When the BESS remains in charge mode for a few time steps, $\frac{\omega_b}{\omega_g}$ decreases again as the SoC rises. In this scenario, $\frac{\omega_b}{\omega_g}$ may fall below R_{th}, causing the BESS to switch back to discharge mode. To prevent this swing between charge and discharge modes, the coefficient K_b must increase with each iteration, which can be implemented using Eq. (5) by adding a constant value ϵ. A higher ϵ reduces the charging/discharging swing but also slows the SoC rise rate. Fig. 3 illustrates the effect on the SoC charge mode for $\epsilon = 0.05$, $\epsilon = 0.09$, and $\epsilon = 0.2$ for a network with two storage units in a specific day. In addition, it shows the SoC balancing strategy, where $n = 5$. Fig. 3 clearly shows that a higher ϵ value leads to smoother charging operation, and more charging/discharging cycles. In the case of $\epsilon = 0.2$, the BESSs have two fully discharging/charging cycles without any ripples in the SoC.

4.4. Feasibility analysis of the optimization program

Batteries are often operated at a fraction of their maximum power to enhance their lifespan, thermal stability, and efficiency. In practice, the operating range is typically between 20% and 80% of the nominal power, but this depends on the specific design and use case.

In addition to battery characteristics, the operational power point depends on both the capacity of RES and the demand level. The goal is to select a maximum charging/discharging power rate for the BESS that prevents curtailment of RES power. As the RES output increases, the BESS must operate at a higher power level to absorb excess energy. Curtailment of RES power can lead to infeasibility in the optimization process, especially if the RES capacity is sufficiently large to supply the load; thus, avoiding curtailment is crucial for system performance. For instance, in an EV parking lot microgrid, that is illustrated and characterized in the section V, with a PV installation capacity of 15 kW, setting the maximum charging power for the BESS to 30% of the nominal maximum helps maintain feasibility in the optimization program for whole a year. In charging mode, a higher RES capacity or a greater maximum charging/discharging power $P_b^{\max}$ accelerates the charging rate, allowing the SoC to reach its upper limit more quickly. When this occurs, any excess RES power may render the program infeasible. Conversely, when demand rises, the BESS maximum charging power or RES capacity may need to increase, and vice versa when demand decreases.

On the other hand, since load changes seasonally in this paper, holding the RES power capacity and maximum charging/discharging power rate at a fixed value, load variations may lead program infeasible. Therefore, three parameters including load demand, RES capacity, and maximum power point that BESS can operates in, are important in feasibility of the optimization program. In addition, the selected value of

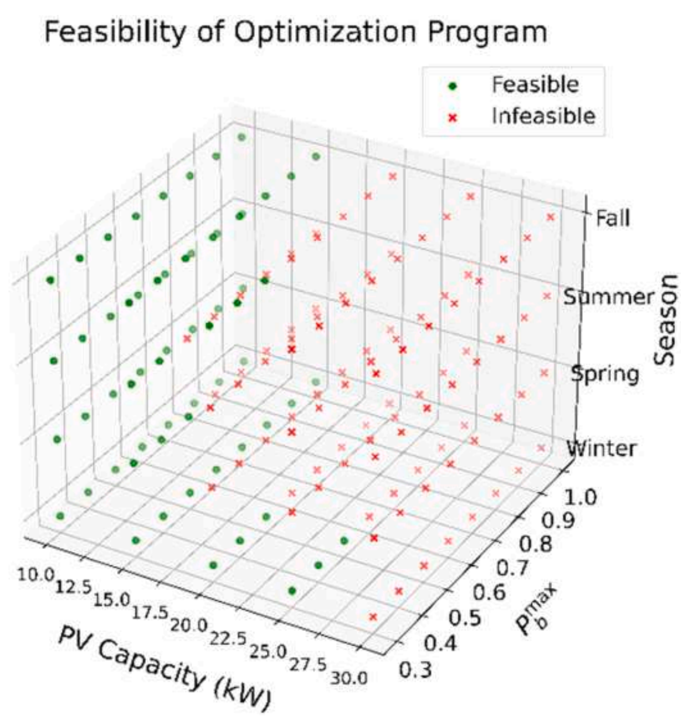

Fig. 4. Feasibility analysis in EV parking lot microgrid.

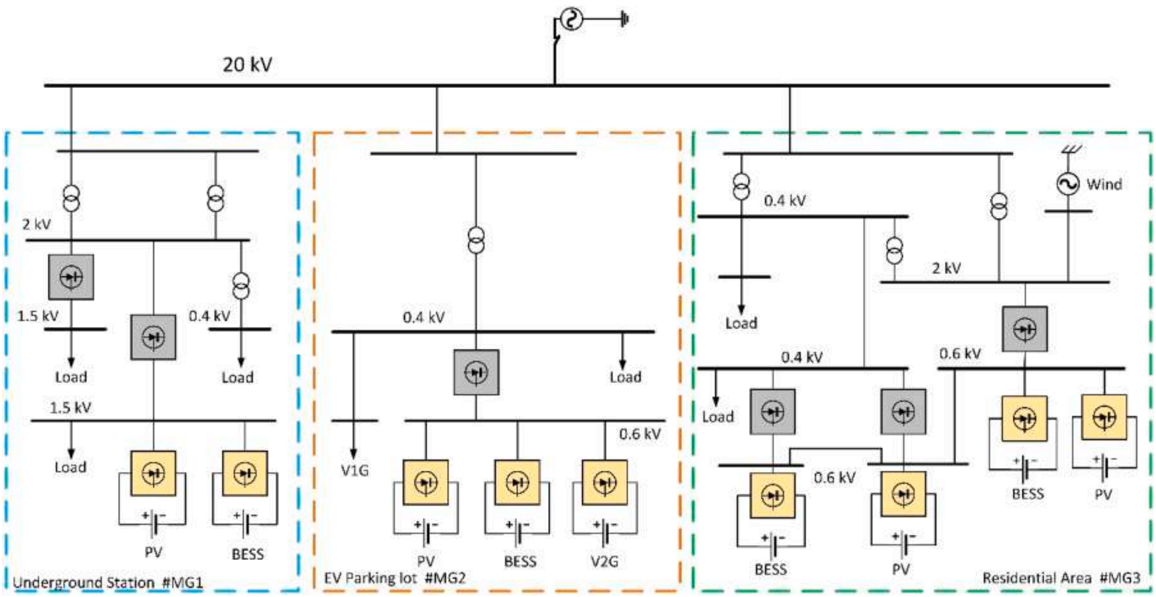

Fig. 5. Case study microgrids.

Table II
parameters and inputs for the microgrids under study.

Inputs	#MG1	#MG2	#MG3
C_{PV} [kW]	109	12	$2*16$
C_{wt} [kW]	0	0	33
V_{DC} [V]	750	300	300
E_b [kWh]	500	50	$2*270$
$P_g^{\max}$ [kW]	1500	45	350
$K(0)$	0.5	0.5	0.5
ε	0.08	0.4	0.5
SoC($t=0$)	0.8	0.9	0.9/0.6
P_l^c [% of P_l]	12	59	60

$P_b^{\max}$ significantly affects the utilization rate of BESSs, renewable energy curtailment, imported grid power, and the resilience performance during islanded operation. To make this fact more visible and quantitatively interpretable, referring to the example above as EV parking lot microgrid, Fig. 4 shows the feasible and infeasible spaces for RES rating power change from 10 to 30 kW, seasonal load changes, and $P_b^{\max}$ between 0.3 and 1 of its rated value $P_{dis}^{\max}$. From Fig. 4, it is clear and expected that for a lower capacity of the PV system, the program remains feasible for all seasons, and the BESS can operate at any percentage of its rated value. On the other hand, the feasibility rate decreases, especially during seasons with higher load demand, such as spring and summer, when PV capacity increases (from 15 to 25 kW). Feasibility is only achieved for lower load demand (winter and fall) if the BESS operates at a lower percentage of its rated power. In the worst case, when the PV power rating exceeds the load demand (30 kW), the program becomes infeasible for any season and at any BESS operating point. Therefore, the adopted $P_b^{\max}$ settings for MG1 and MG2 were selected from feasible operating regions that ensure feasible optimization solutions for all generated seasonal scenarios while maintaining acceptable BESS utilization and power dispatch performance. Note that the program is considered feasible in this analysis only if it is feasible for all scenarios produced in Section III, whereas sometimes the program is feasible only for some scenarios. This means that the produced scenarios may be another factor affecting feasibility.

5. Case studies description

In this section, three microgrids are illustrated and characterized. Fig. 5 shows these microgrids connected to the main grid. The three microgrids include an underground station (#MG1), a parking lot for EVs (#MG2), and a residential area (#MG3), all connected to the point of common coupling (PCC) at a 20 kV bus. The microgrids feature various voltage levels in both AC and DC subgrids, as depicted in Fig. 5. Photovoltaic (PV) systems are connected to the DC bus through inverters, while BESSs are linked to the DC bus via bidirectional AC/DC converters. Each DC subsystem is interconnected with an AC subsystem using bidirectional

AC/DC converters. Both underground station and the parking lot include a PV system and a BESS, while the residential area hosts two PV systems, two storage units, and a wind turbine system. The parameters and characteristics of these systems, which were modeled and formulated in the first part, are listed in Table II as inputs for the optimization program. Additional data on the capacity of PV, wind, and storage systems, as well as the daily total and critical supply for these three microgrids, is available and imported from the authors' previous works [38–41].

Using the data in Table II, other inputs required for the program can

Fig. 6. Average daily load for the three microgrids. (a) Underground station, (b) Parking lot, (c) Residential area.

Table III
Summary statistics of climatic data in each scenario and season.

Winter			
Scenario	Temperature	Wind Speed	Solar Irradiance
	[°C]	$[m/s]$	$[W/m^2]$
Baseline scenario	10.84 ± 1.81	3.40 ± 0.59	171.60 ± 239.05
Increased temperature	14.17 ± 2.54	3.40 ± 0.59	171.60 ± 239.05
Reduced solar irradiance	10.84 ± 1.81	3.40 ± 0.59	43.87 ± 78.38
Increased wind speed	10.84 ± 1.81	6.52 ± 1.84	171.60 ± 239.05
Reduced wind speed	10.84 ± 1.81	1.23 ± 0.57	171.60 ± 239.05
Spring			
Scenario	Temperature [°C]	Wind Speed $[m/s]$	Solar Irradiance $[W/m^2]$
Baseline scenario	17.03 ± 3.94	2.44 ± 0.59	265.75 ± 320.84
Increased temperature	21.20 ± 5.00	2.44 ± 0.59	265.75 ± 320.84
Reduced solar irradiance	17.03 ± 3.94	2.44 ± 0.59	105.45 ± 160.76
Increased wind speed	17.03 ± 3.94	4.60 ± 1.53	265.75 ± 320.84
Reduced wind speed	17.03 ± 3.94	1.31 ± 0.67	265.75 ± 320.84
Summer			
Scenario	Temperature [°C]	Wind Speed $[m/s]$	Solar Irradiance $[W/m^2]$
Baseline scenario	24.81 ± 2.51	2.08 ± 0.71	285.33 ± 343.80
Increased temperature	28.04 ± 3.45	2.08 ± 0.71	285.33 ± 343.80
Reduced solar irradiance	24.81 ± 2.51	2.08 ± 0.71	166.69 ± 234.04
Increased wind speed	24.81 ± 2.51	3.88 ± 1.53	285.33 ± 343.80
Reduced wind speed	24.81 ± 2.51	1.25 ± 0.71	285.33 ± 343.80
Fall			
Scenario	Temperature [°C]	Wind Speed $[m/s]$	Solar Irradiance $[W/m^2]$
Baseline scenario	16.38 ± 3.44	2.93 ± 0.56	176.59 ± 247.69
Increased temperature	19.13 ± 3.80	2.93 ± 0.56	176.59 ± 247.69
Reduced solar irradiance	16.38 ± 3.44	2.93 ± 0.56	49.85 ± 100.65
Increased wind speed	16.38 ± 3.44	5.93 ± 1.62	176.59 ± 247.69
Reduced wind speed	16.38 ± 3.44	1.15 ± 0.60	176.59 ± 247.69

be easily calculated based on the corresponding equations in Sections II and IV. The upper and lower bounds for the SoC, the discharge/charge efficiency of the BESS converter, the off-set SoC, and the required time for full charge are 0.2, 0.9, 1, 0.4, and 4 h, respectively. Fig. 6 illustrates the daily total

load for each microgrid, calculated as the average of the yearly load profile, whereas the proposed numerical calculations take into account the exact seasonal load data. It is worth mentioning that all available data has been recorded in 15-minute time slots; therefore, a day's simulation is divided into 96 time steps.

6. Scenarios generation for the case studies

Climatic data consist of hourly solar irradiance, wind speed and ambient temperature, collected in Palermo (Italy) between 2017 and 2021. The resampling moving-window block bootstrap methodology ([42,43]) is applied with window width $\delta_t = 10$ in order to generate $n_B = 100$ synthetic series of each environmental factor (see Algorithm 0).

The environmental-based energy scenario, defined on the base of each empirical distribution, are described in section III: "scenario mean", "scenario high temp", "scenario low solar", "scenario high wind", "scenario low wind". Notice that, for each scenario, only the target external influence changes while the others remain at an average value to isolate effects.

Table III collects mean and variability values of each renewable source with respect to each scenario and season. These summary statistics highlight the expected seasonal variations in temperature, wind speed, and solar irradiance across the defined scenarios. Temperature follows a clear seasonal pattern, reaching its peak in summer and its lowest values in winter, with higher variability observed in warmer seasons. The increased temperature scenario shows a consistent increment on the mean and variability. Wind speed exhibits lower mean values in summer and spring, while the highest variability in the baseline scenario is recorded in summer. The increased wind speed scenario results in almost a twofold increase compared to the baseline, while the reduced wind speed scenario shows a significant decrease, particularly in winter and fell, where the mean drops to nearly 1 m/s. Solar irradiance follows a strong seasonal trend, with maximum values in summer and minimum in winter. The reduced solar irradiance scenario shows a notable decline across all seasons, with winter experiencing the most extreme reduction due to already low baseline values.

Overall, the bootstrap method effectively captures seasonal variability while maintaining realistic fluctuations in climatic data. These results indicate that the generated inputs reflect the typical dynamics of renewable resource variability, while approximating more extreme operating conditions, thus providing a reliable basis for assessing the impact of environmental variations on AC/DC microgrids. In particular, the approach offers consistent and computationally efficient inputs for scenario-based simulations, supporting both operational planning and reliability analysis under normal operating conditions.

7. SIMULATION ANALYSIS AND DISCUSSION

To gain a better understanding of how the proposed security-based optimization and external weather parameters affects battery utilization and reliability indices in on-grid and islanded modes, two cases are analyzed: Case 1 considers both minimizing power imported from the main grid and maintaining sufficient SoC for islanded mode, referred to as the security-based case. Case 2 represents the non-secure scenario, where Eq. (17) and the second term in Eq. (2) are removed from the program.

It should be noted that the primary contribution of this work is the development of a resilience-oriented day-ahead EMS framework integrating adaptive SoC-aware scheduling, seasonal renewable scenario analysis, and islanded operation assessment for AC/DC microgrids, rather than proposing a new optimization solver. Since many existing studies adopt different operational objectives, control structures, uncertainty models, and network configurations, direct quantitative comparison under identical conditions is not straightforward. Therefore, the effectiveness of the proposed framework is evaluated through comprehensive scenario-based analyses considering different seasonal conditions, microgrid structures, BESS operating limits, and islanded operating scenarios.

7.1. Security-based case

In this subsection, both on-grid and off-grid operation modes are evaluated for the three microgrids shown in Fig. 5. The objective of this paper is to analyze how various external condition scenarios for RESs, driven by environmental factors discussed in Section III of the first part, affect storage utilization in the proposed optimization program and resilience in islanded mode through reliability indices measurements. As stated in the first part of the paper, the scenarios are categorized into five labels, defined in a list as $S =$ {"scenario mean", "scenario high temp", "scenario low solar", "scenario high wind", "scenario low wind"}. To achieve this, the daily SoC variations are depicted for one month representing each season across the three microgrids: January (winter), May (spring), August (summer), and November (fall). In this case, to achieve program feasibility, the maximum operating charging/discharging power $P_b^{\max}$ is set to 50% of its maximum allowable value $P_{dis}^{\max}$ in #MG1 for all seasons. However, in summer, the program is feasible only if $P_b^{\max}$ is 100% of $P_{dis}^{\max}$. In #MG2, $P_b^{\max}$ is set to 30% of $P_{dis}^{\max}$ in summer and 50% for the other seasons. Finally, in #MG3, setting $P_b^{\max} = 0.3P_{dis}^{\max}$ ensures efficient and feasible BESS utilization throughout the year.

Given the #MG1 (underground station), the SoC changes in a day and PV output power for four months mentioned above are depicted in Fig. 7(a) and (b) respectively. Note that since the PV system is the only RES in MG1 and MG2, only the first three scenarios in the set S are

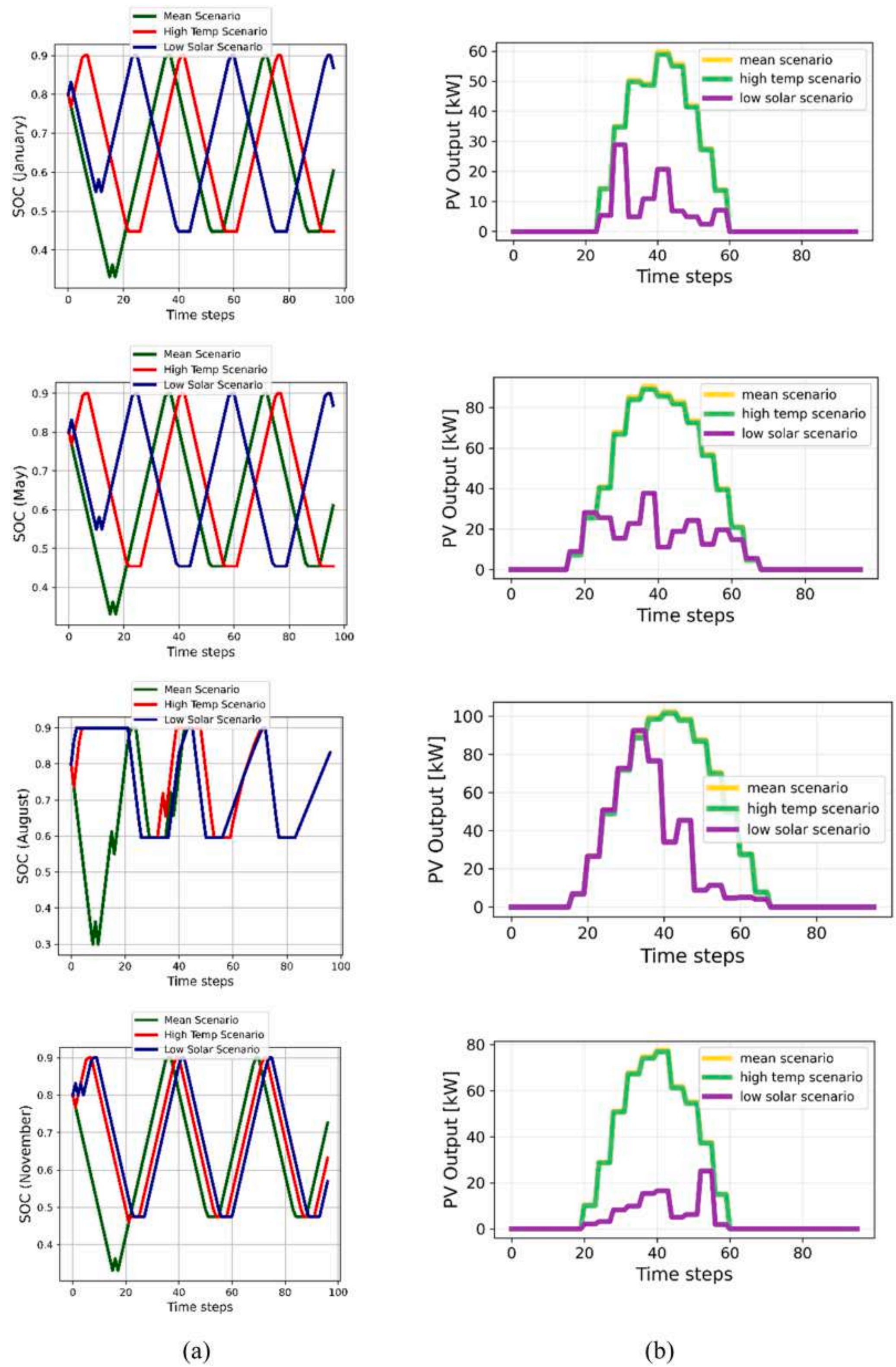

Fig. 7. (a): Daily SoC changes, and (b): PV output power in various seasons for given scenarios in #MG1.

considered.

Fig. 7(a) illustrates the daily SoC changes. It is evident that the SoC trends for winter, spring, and fall are nearly identical. This similarity occurs because the capacity of the PV systems in #MG1 is much lower than the load demand, which minimally affects the operating cycle. in fact, the rate of PV capacity C_{PV} to maximum load demand is 7.8%. In general, after $t = 20$, as the load increases substantially, the minimum SoC rises due to security constraints that ensure critical loads are supplied for at least three time steps. In contrast, during summer, the higher power generation from the solar systems results in a shorter SoC fluctuation interval, thereby increasing the number of charging/discharging cycles, which could reduce battery lifetime.

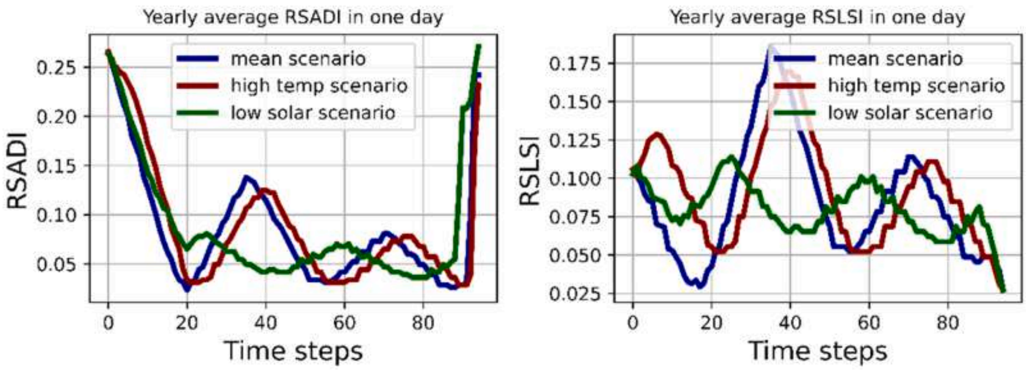

Fig. 8. Average daily reliability indices for #MG1.

Regarding the external conditions represented by the three scenarios; mean, high temperature, and low solar. Fig. 7(b) shows that during the early hours of the day, the program selects the discharge operation mode under the mean scenario across all seasons. However, in the high temperature scenario, the battery first charges before discharging. Furthermore, Fig. 7(b) depicts the power output of the PV system across different seasons for the three scenarios. Although the power generated under the mean scenario is slightly higher than that of the high temperature scenario, the program adopts different charging/discharging strategies, especially during the early hours. This difference causes a shift in the charging/discharging cycles, which in turn affects the resilience observed at each hour. This shift is particularly noticeable between the mean, high temperature, and low solar scenarios during both winter and spring. For example, at $t = 38$, the SoC nearly reaches its maximum in the mean and high temperature scenarios, while it approaches its minimum in the low solar scenario. Consequently, if a fault occurs at this time, forcing the microgrid into islanded mode, the first two scenarios would be able to supply the critical load for a longer duration, leading to higher reliability indices and better resilience.

Fig. 8 illustrates the daily average values of the Renewable and Storage Availability Duration Index (RSADI) and the Renewable and Storage Load Supply Index (RSLSI) as reliability indices for different external condition scenarios over a year. These indices are calculated as Eq. (30) and Eq. (31).

In the early hours, since the PV system's output power is zero and the SoC is at a high level, RSADI drops sharply from its maximum point, reducing BESS availability. Meanwhile, RSLSI directly fluctuates based on SoC variations. For instance, in the scenario mean, RSLSI decreases in the early hours as SoC drops, whereas in the high temperature scenario, RSLSI increases due to a rise in SoC. A general observation is that the reliability indices for both the scenario mean and high temperature scenarios are higher than those for the low solar scenario, although the latter may occasionally exhibit higher values at certain hours. This suggests that higher renewable energy availability may enhance the reliability of the microgrid.

The same results for MG2 are illustrated in Fig. 9, which includes only PV systems and one BESS. Based on Fig. 6 and Table II, unlike MG1, the maximum load demand in MG2 occurs during the early and late hours of the day, with the minimum demand at noon as EVs are out of the parking lot. Additionally, the PV capacity in MG2 is relatively significant compared to the demand, with a ratio of 37.5% to the maximum power demand. Looking at Fig. 9(a), during the early hours, as load demand decreases and PV power is unavailable, SoC starts dropping to reduce operational costs, as defined by Eq. (2). This trend is consistent across all three scenarios since no PV power is generated during this period. In winter, spring, and fall, SoC follows a similar pattern of changes. During these seasons, when PV output reaches its peak at noon, SoC in the scenarios mean and high temperature drops with a delay compared to the low solar scenario, as higher PV generation can still meet the load demand. This results in a noticeable shift in charging and discharging cycles. However, in summer, due to higher PV generation, BESS begins its first charging cycle earlier since both PV and BESS can still meet the demand, further reducing operational costs. As a result, in summer, the number of charging/discharging cycles decreases, which helps extend BESS lifespan.

The daily average reliability indices for #MG2 are plotted in Fig. 10. It is evident that these indices peak twice during the day, as SoC reaches its maximum value twice, according to Fig. 9(a). The first peak is significantly higher than the second one since, during the first peak, both PV and BESS operate at full capacity, whereas in the late hours, only BESS is fully charged, and PV is unavailable. As expected, in general, the scenarios mean and high temperature demonstrate higher reliability. However, in the late hours, the reliability indices for the low solar scenario surpass those of the other two scenarios due to the previously mentioned charging/discharging shift. At this interval, for example at $65 \leq t \leq 80$, SoC is higher than in the other scenarios, while PV power remains limited.

Fig. 11 illustrates SoC variations in #MG3 in January (Winter) for the five given scenarios in the set S, considering the presence of a wind turbine system in addition to two PV generation systems. Since similar results were observed across other seasons and there is a page limit, we only show daily SoC changes for winter. The following explains why the given scenarios across different seasons may not meaningfully affect SoC variations. In this case, the RES capacity to maximum load demand ratio is 26%. The renewable power generation for these five scenarios across different seasons is shown in Fig. 12. Notably, when analyzing a given scenario for one renewable system, the power output of the other RES remains fixed at its mean value. For instance, in the low solar scenario, the wind system generates its mean value at each time step. Additionally, according to Fig. 12, in the high wind scenario, wind system generation in winter and fall drops to zero due to excessively high wind speeds exceeding the cut-off threshold, leading to a complete halt in power generation. Given these two factors, in certain seasons, RES generation in the low solar scenario can surpass that in the high wind scenario.

However, based on Fig. 11, the given scenarios across different seasons do not significantly affect SoC variations. This is because, during the early hours, when load demand is low, RESs and BESSs tend to supply a large portion of the load, regardless of whether RES generation is available or not, in order to reduce operational costs. Later in the day, when RES generation reaches its maximum (in most cases) and the SoC of storage systems is at its minimum, BESSs begin charging according to the charging algorithm introduced in the first part of the paper. This charging/discharging process is gradually adjusted, minimizing the number of cycles. In this microgrid, the process stabilizes at two cycles, which represents the most efficient operation for BESSs. From Fig. 11, it is evident that the SoC balancing strategy, as introduced in Section IV of the first part, is successfully achieved. The two BESSs begin discharging

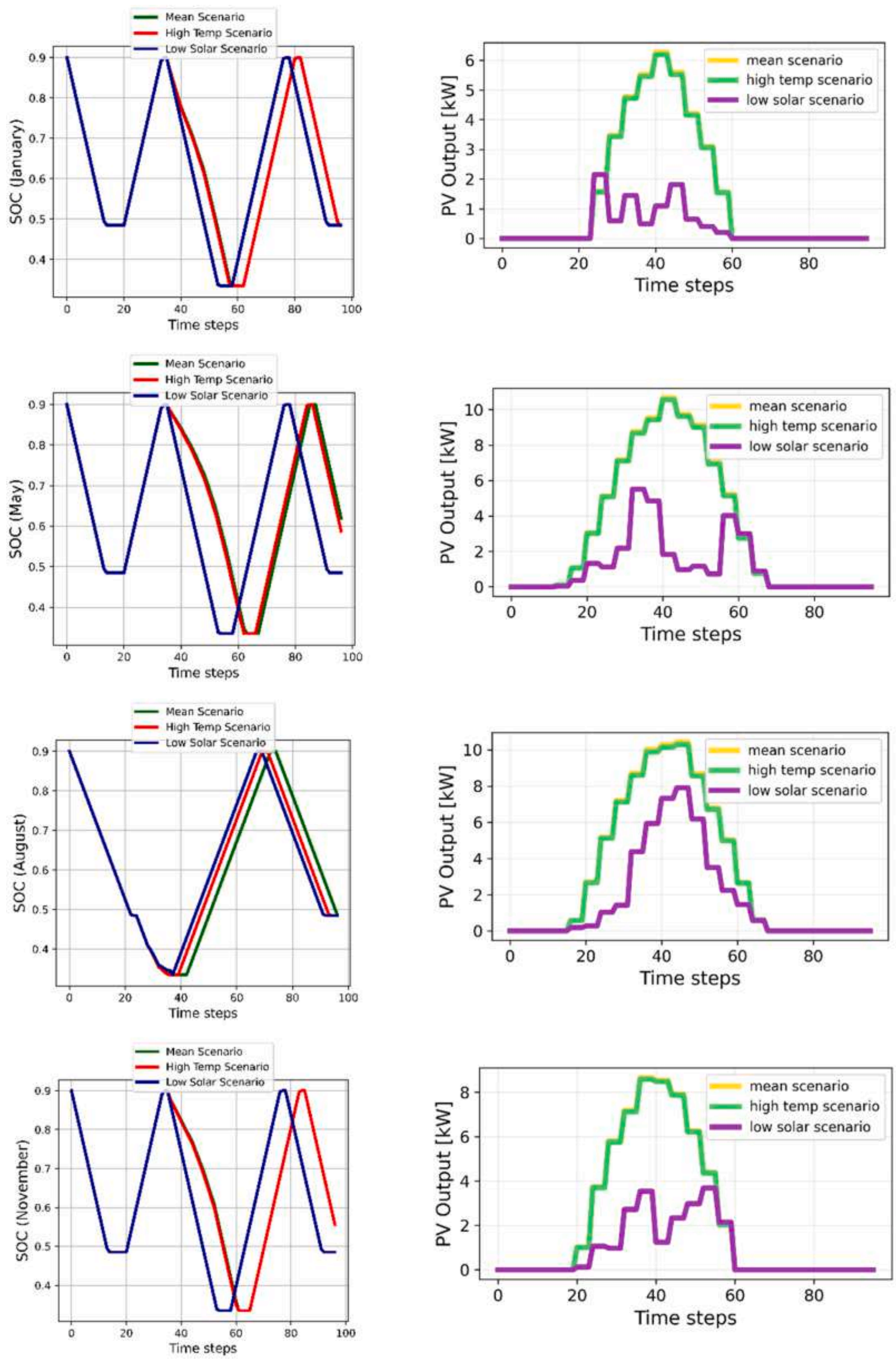

(a) (b)

Fig. 9. (a): Daily SoC changes, and (b): PV output power in various seasons for given scenarios in #MG2.

with initial SoC values of 0.9 and 0.6, respectively, at $t = 0$, and their SoC converge at $t = 25$. Notably, a higher exponent factor n in Eqs. (24), (25), and (27) results in faster SoC convergence. However, this can also lead to an increase in charging/discharging cycles, which may shorten battery lifespan and, in some cases, even render the optimization program infeasible.

Fig. 13 illustrates the average reliability indices for #MG3 over a year under the five given scenarios. It is evident that external weather conditions affecting PV systems, while maintaining normal conditions for the wind system, result in a more resilient operation in islanded

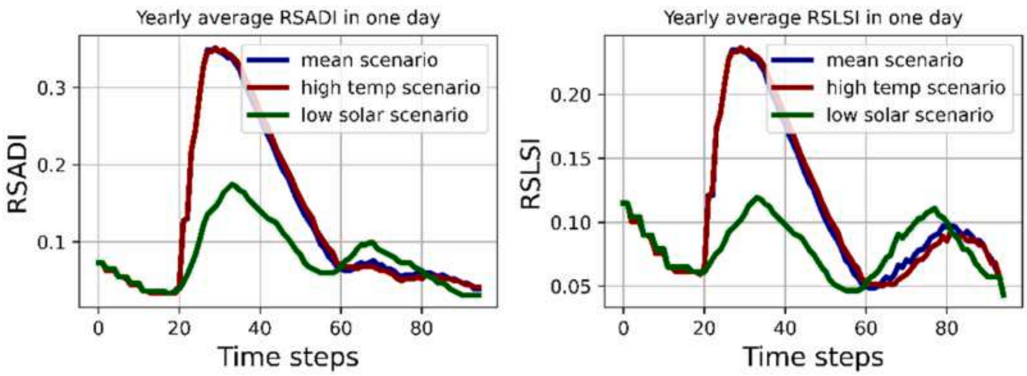

Fig. 10. Average daily reliability indices for #MG2.

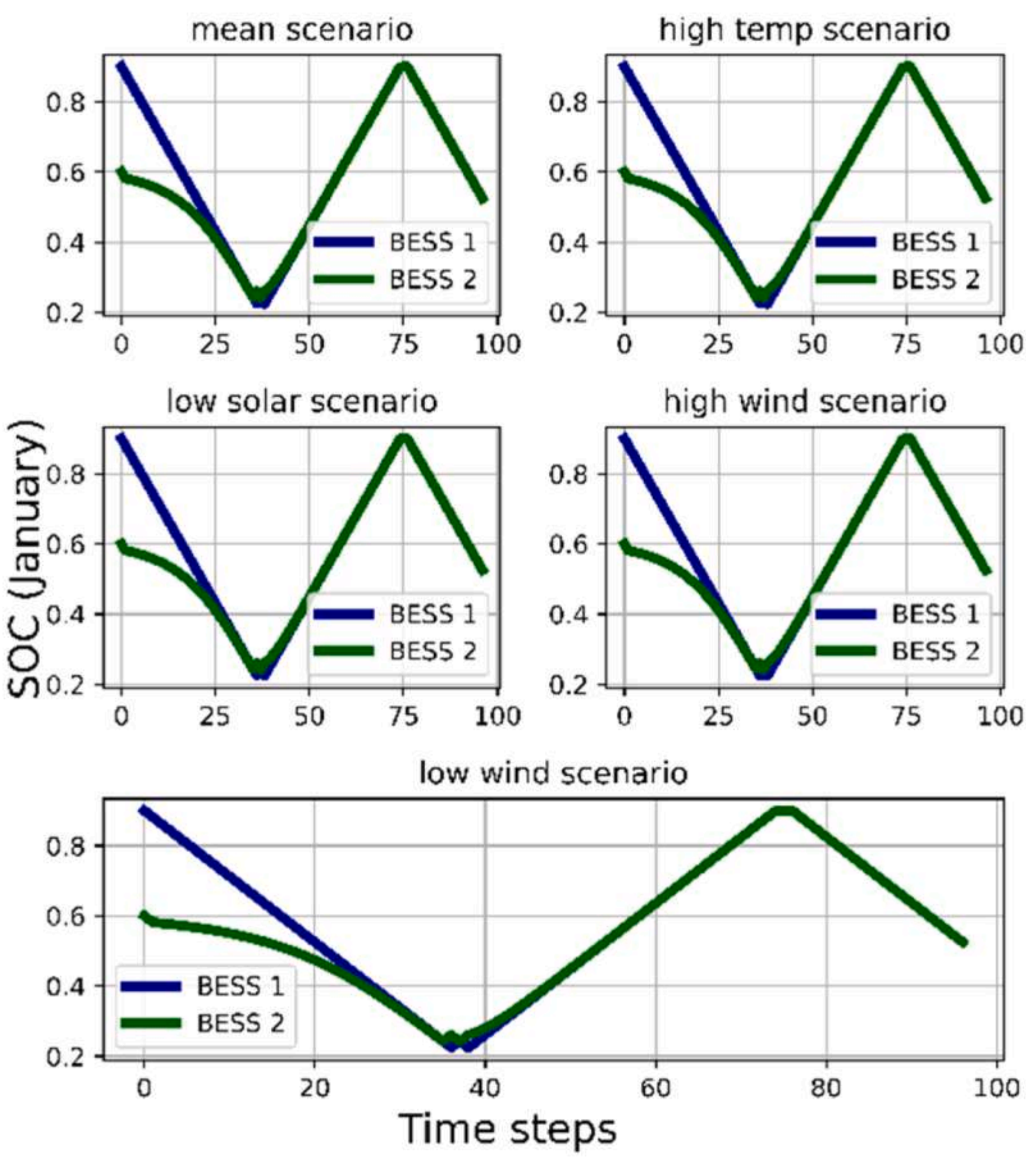

Fig. 11. Daily SoC changes in winter for given scenarios in #MG3.

mode compared to scenarios with intensive wind conditions (i.e., high wind and low wind scenarios). This suggests that extreme variations in wind speed, whether excessively high or low, can negatively impact microgrid resilience, whereas stable PV generation contributes to more reliable operation. However, considering normal conditions for both PV and wind systems results in an acceptable resilience operation, as expected. This is because an increase in RES generation capacity naturally enhances microgrid reliability, ensuring a more stable and sustained power supply in islanded mode.

To analyze SoC behavior for both BESSs in MG3 under islanded

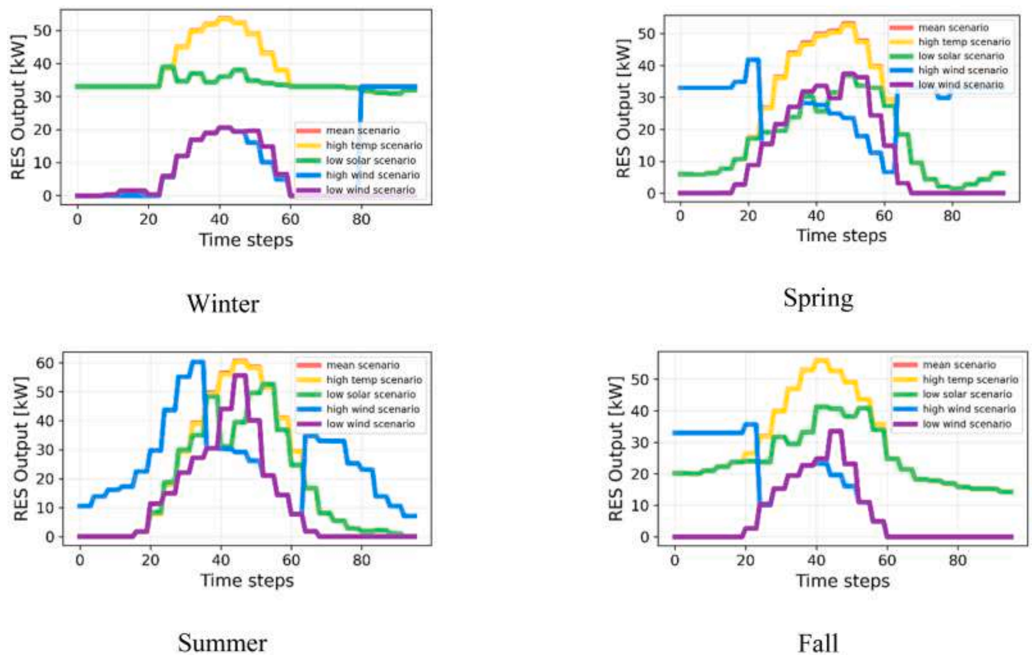

Fig. 12. Power generation of RESs in #MG3.

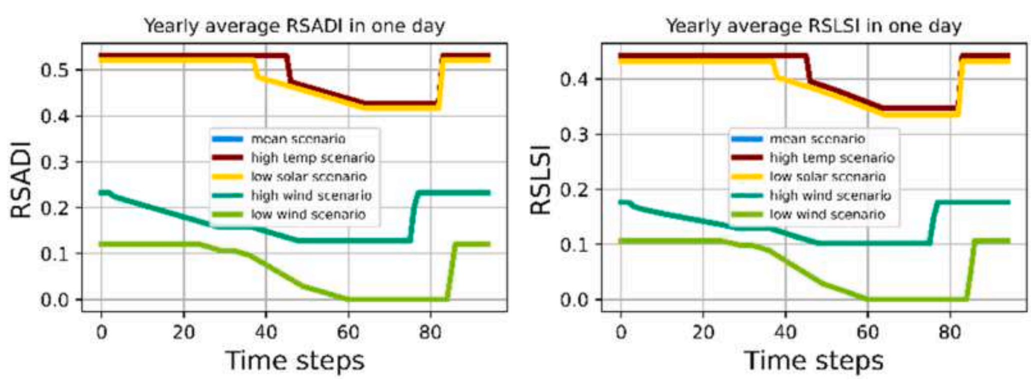

Fig. 13. Average daily reliability indices for #MG3.

mode, a fault must be implemented at a fixed time, following the supply and SoC balance strategies proposed in Subsection B of Sections II and IV, respectively, in the first part of the paper. Fig. 14(a) and (b) illustrate the SoC changes after a fault at $T_f = 20$ and $T_f = 40$, respectively, during winter. Before the fault occurs, SoC follows the same trend as in on-grid mode. Notably, even in islanded mode, the SoC balancing strategy remains valid. SoC balancing is applied in the charging mode for scenarios mean, high temp, and low solar. Conversely, SoC balancing is achieved in the discharging mode for scenarios high wind and low wind. Additionally, Fig. 14 shows that SoC reaches its minimum value in the high wind and low wind scenarios, confirming a worse resilience operation compared to the first three scenarios.

7.2. Non-secure case

To evaluate the efficiency of the proposed operation algorithms in terms of resilience and reliability, it is necessary to analyze the non-secured mode, where storing the minimum required energy in BESS, ensuring supply for at least three time steps in islanded mode, is not mandatory. As a result, in the non-secure case study, the objective function in Eq. (2) includes only the first part related to operation cost, removing the requirement to maintain stored energy. Eq. (17) is also excluded from the program, meaning the system is optimized purely for cost efficiency without explicitly considering energy reserves for islanded mode. This comparison helps assess the trade-off between economic operation and resilient microgrid performance under different operational scenarios.

The non-secure program is implemented in #MG1, #MG2, and #MG3. In this mode, the SoC behavior follows a simple pattern. The BESS starts discharging from the first time step, prioritizing immediate cost minimization. Then, SoC reaches its minimum level quickly and remains there for the rest of the day, as there is no requirement to store energy for islanded operation. Due to this predictable and trivial SoC trend, SoC changes are not shown here. However, to assess the impact of security constraints on system resilience, average reliability indices are presented and compared with those from the security-based case. This allows for a clear evaluation of how ensuring minimum stored energy improves microgrid reliability and resilience.

Fig. 15 depicts the reliability indices on average over a year for #MG1, #MG2, and #MG3. Fig. 15(a) shows RSADI and RSLSI indices for #MG1. Comparing this plot to that in Fig. 8, it is concluded that although SoC reaches its minimum value at $t = 35$, BESS and RES are not available anymore from $t = 20$, decreasing the resilience. The same analysis is true for #MG2, where a sharp drop in reliability indices is visible by comparing Fig. 15(b) to Fig. 10. However, considering both Fig. 15(c) and Fig. 13 simultaneously, it is clear that non-secure

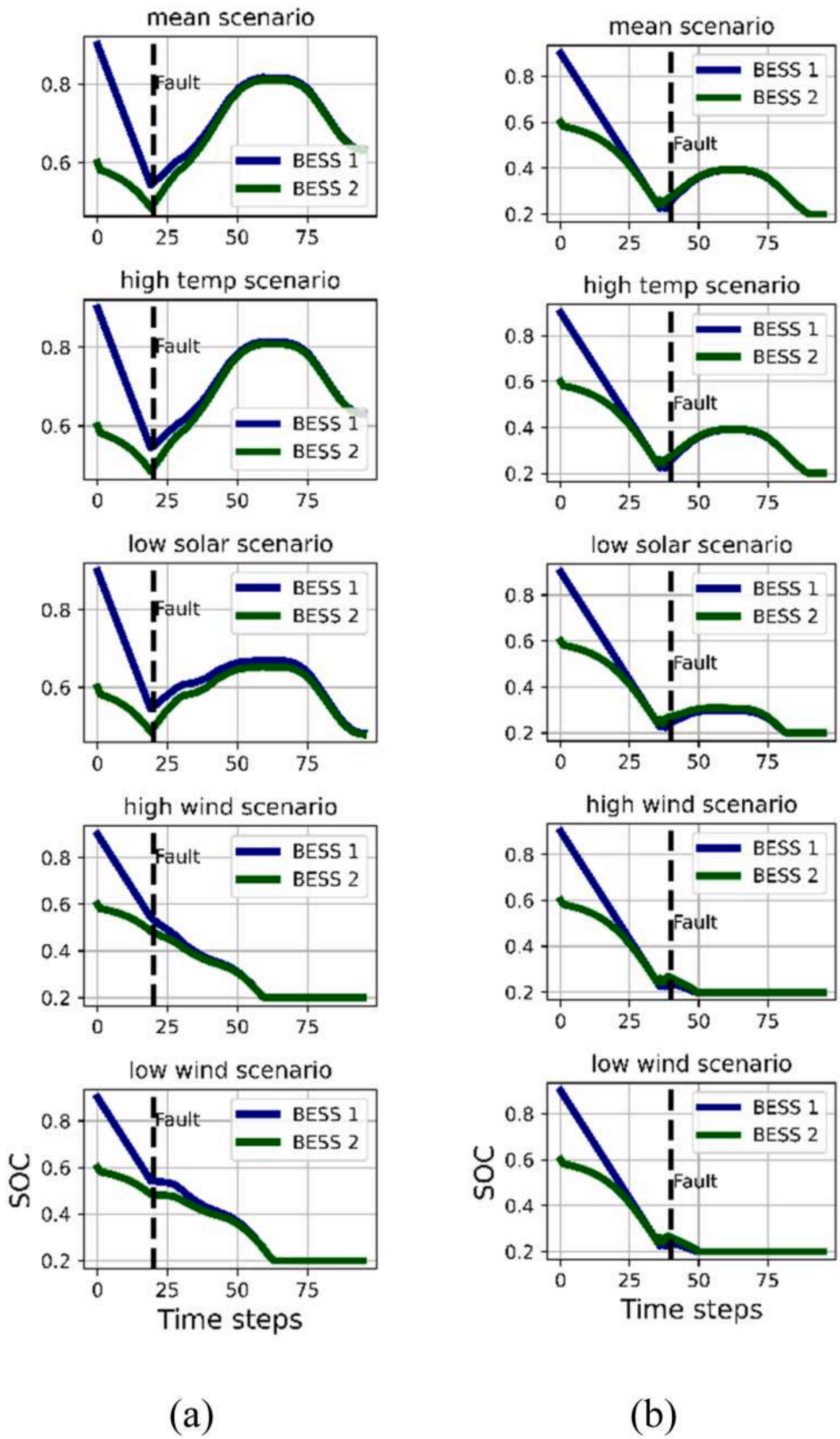

Fig. 14. Islanded mode analysis in #MG3. (a): $T_f = 20$, and (b): $T_f = 40$.

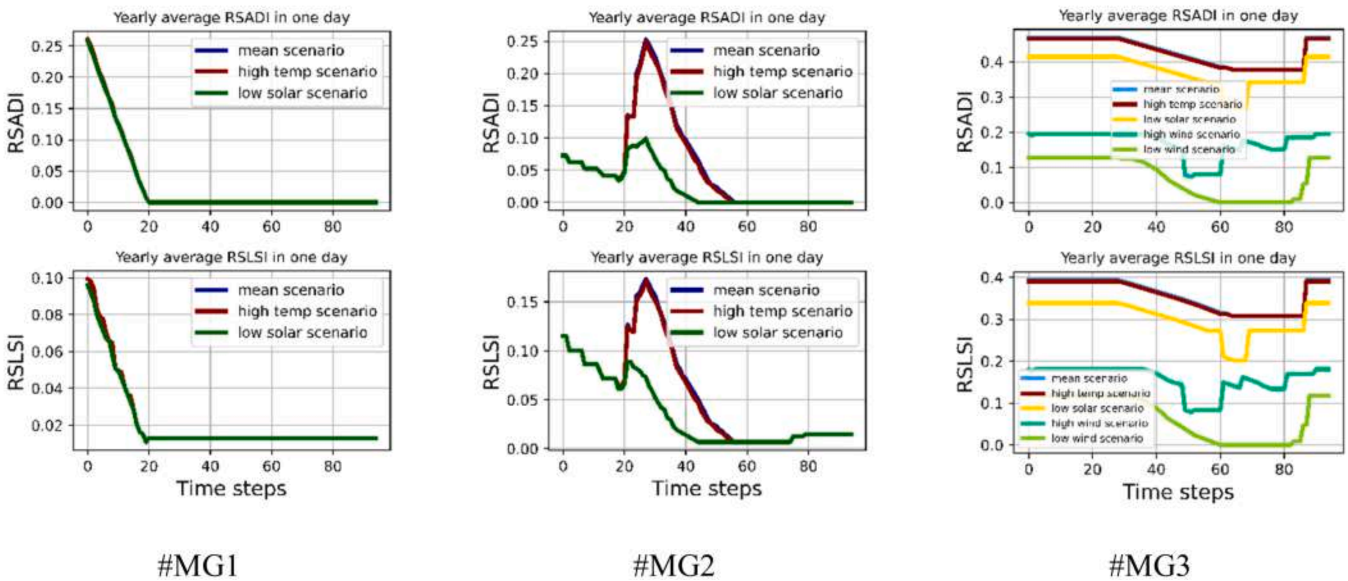

Fig. 15. Reliability indices for three microgrids in non-secure case.

operation mode has not reduced reliability indices meaningfully in #MG3. RSADI and RSLSI decrease by a maximum of 18% in the low solar scenario and a minimum of 12% in the low wind and high wind scenarios.

However, in the non-secure case, it would be interesting to analyze the SoC trend after a fault. Similar to the analysis done for #MG3 in subsection *A*, a fault is applied to the PCC point between the main grid and #MG3, causing #MG3 to operate in islanded mode. Fig. 16 shows the SoC changes after $T_f = 20$ and $T_f = 40$. Based on Fig. 16 and Fig. 14, it is clear that load supply by RESs and BESSs follows a similar trend, meaning the security-based case is slightly better than the non-secure mode, though the difference is negligible. This proves the fact that if there is sufficient RES capacity, security constraints like storing the required energy at BESSs may not be necessary. In addition, SoC balancing after a fault remains valid even in the non-secure operation mode.

8. Conclusion

The methodology for optimal power dispatch in renewable-storage AC/DC hybrid microgrids, operating in both grid-connected and islanded modes, is presented in this paper. The mathematical models for mixed-integer linear programming are formulated to minimize operational costs while maximizing the required energy stored in BESSs. The importance weights of these two objective variables are tuned so that BESSs begin discharging when fully charged and start charging when they reach the minimum required level to meet demand over three time intervals in islanded mode. To achieve this, an incremental charging adjustment factor (ϵ) was introduced in charging mode. It was shown that a higher ϵ not only reduces charging/discharging swings but also accelerates SoC rise rate, which can prolong battery lifetime. However, ϵ should be carefully determined, as a higher value may render the program infeasible in cases of renewable power curtailment. Additionally, the impact of various parameters, such as seasonal changes, renewable capacity, and the maximum discharging power rate of BESSs, on program feasibility was discussed. Furthermore, in both on-grid and off-grid operating modes, an SoC-based technique is adopted to achieve SoC balancing, which increases the lifecycle of the storage system when multiple BESSs are present. To evaluate the influence of renewable power uncertainty, a data-driven algorithm predicts RES output power based on five years of historical environmental parameters to evaluate the effect of five external conditions, scenarios "mean," "high temp," "low solar," "high wind," and "low wind", on the proposed operation methodology, modeled through time series methodologies in order to preserve their key statistical properties such as seasonality and short-term dependencies. The proposed framework, while not designed to replicate extreme events, provides a reliable and efficient tool for routine monitoring and planning under normal conditions, offering actionable insights for maintenance, storage optimization, and policy decisions on sustainable energy management. Based on the three microgrids mentioned as case studies, the key findings of the simulation results are as follows:

- RES generation for the given scenarios shows how external conditions can influence SoC trends in all microgrids. In addition, it is notable that, in the secure-based case, higher RES capacity may lead to smaller SoC deviations, resulting in lower charging/discharging cycles at BESSs, which in turn improves battery lifetime and utilization. However, In the non-secure case study, the BESSs' SoC decreases rapidly and reaches its minimum allowable limit (SoC = 0.2) to reduce operating costs and does not recharge afterward, leading to inefficient battery operation.
- It is proven that external conditions that generate more power generally achieve higher resilience and reliability on average, as measured through RSADI and RSLSI indices. However, the worst scenarios can lead to more resilient operation at specific times due to the BESS operation point before islanding. For example, although the low solar scenario results in lower overall resilience compared to the mean and high temp scenarios, it occasionally exhibits greater reliability factors. However, in #MG3, results show that extreme external conditions, such as high wind and low wind, lead to zero wind system output power at certain hours, resulting in less resilient operation even compared to the low solar scenario.
- Reliability analysis indicates that the security-based operation mode leads to significantly higher reliability and resilience compared to the non-secure operation mode, especially in #MG1 and #MG2, which rely solely on PV systems and have no power availability during early and late hours of the day. However, in #MG3, where a wind system is present alongside PV systems, reliability in the non-secure case decreases by only 12–18%, demonstrating that greater RES availability can enhance reliability regardless of security constraints.
- The SoC balancing strategy is effectively adopted in both islanded and grid-connected modes, ensuring sufficient SoC convergence in

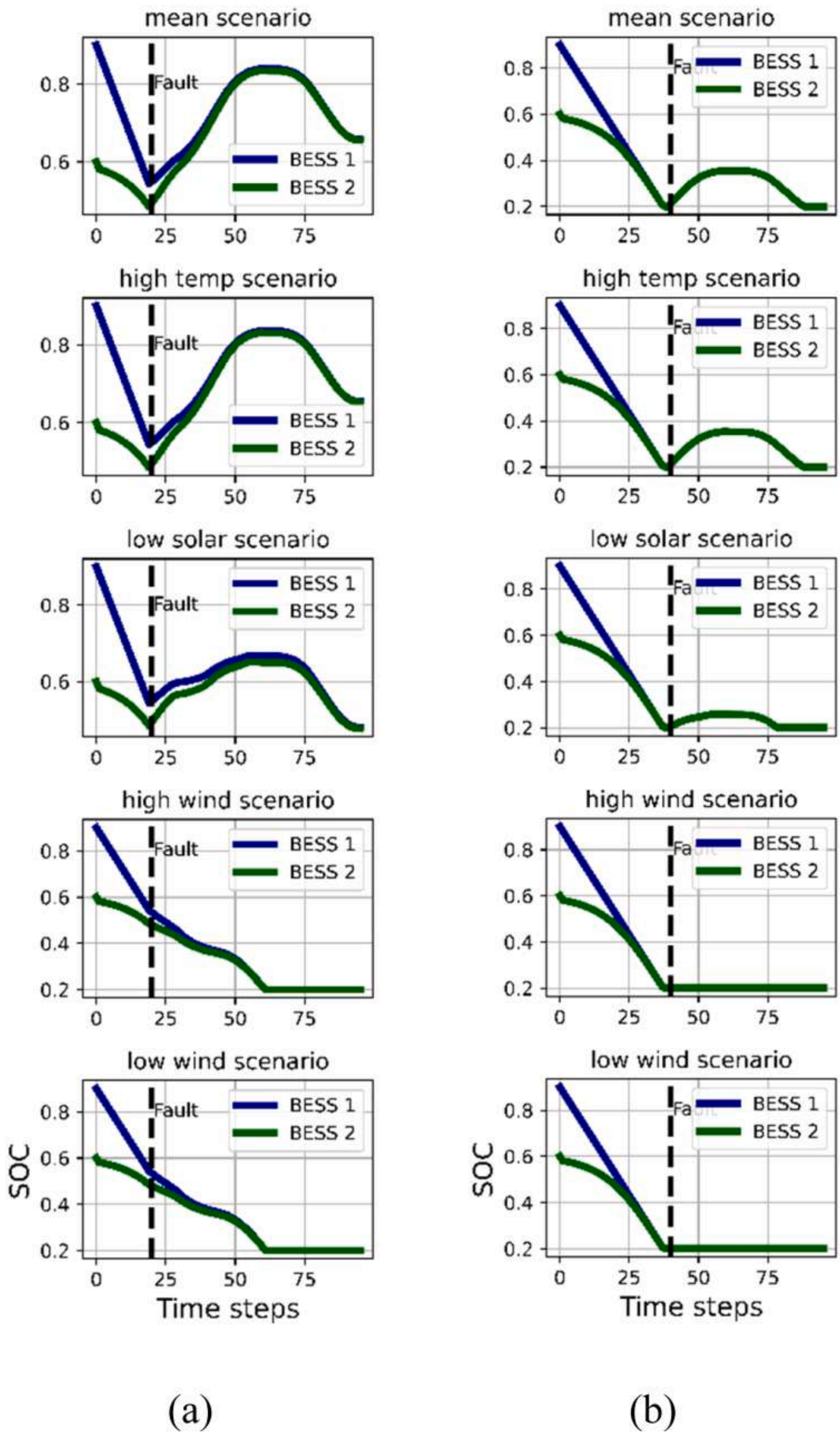

Fig. 16. Islanded and non-secure mode analysis in #MG3. (a): $T_f = 20$, and (b): $T_f = 40$.

both charging and discharging operation modes. It was also shown that SoC balancing remains valid even in the non-secure case. This strategy can contribute to increasing battery lifetime by minimizing excessive charging/discharging cycles.

Despite the promising results, several limitations of the proposed framework should be acknowledged. First, the methodology adopts a simplified MILP formulation and does not explicitly model nonlinear battery degradation mechanisms or detailed converter performance characteristics, which may influence long-term operational behavior. Second, the environmental-based renewable generation scenarios are derived from historical data through bootstrap resampling and are intended to preserve realistic statistical properties under normal operating conditions; therefore, rare extreme events or previously unobserved operating conditions are not explicitly represented. In addition, the feasibility and performance of the optimization framework depend on parameters such as RES capacity, load demand, and BESS charging/discharging operating limits, as discussed in the feasibility analysis. Future work will focus on extending the proposed methodology toward more detailed battery aging models, improved uncertainty representation for extreme operating conditions, and real-time or adaptive energy management implementations for large-scale hybrid microgrid systems.

CRediT authorship contribution statement

Mariano Giuseppe Ippolito: Project administration, Resources, Supervision. **Andrea Marletta:** Visualization, Software, Methodology, Data curation, Conceptualization. **Giulia Marcon:** Writing – original draft, Visualization, Software, Methodology, Data curation, Conceptualization. **Salar Moradi:** Writing – original draft, Visualization, Software, Methodology, Data curation, Conceptualization. **Salvatore Favuzza:** Supervision, Resources, Project administration. **Fabio Massaro:** Supervision, Resources, Project administration. **Gaetano Zizzo:** Supervision, Resources, Project administration.

Declaration of Competing Interest

The authors declare that they have no known competing financial interests or personal relationships that could have appeared to influence the work reported in this paper.

Data Availability

Data will be made available on request.

References

[1] K. Trivedi, Reliability and availability assessment, IEEE Trans. Rel (2023).
[2] Z. Liang, H. Chen, X. Wang, S. Chen, C. Zhang, Risk-based uncertainty set optimization method for energy management of hybrid ac/dc microgrids with uncertain renewable generation, IEEE Trans. Smart Grid 11 (2) (2019) 1526–1542.
[3] M.Y.A. Khan, H. Liu, Y. Zhang, J. Wang, Hybrid ac/dc microgrid: Systematic evaluation of interlinking converters, control strategies, and protection schemes: A review, IEEE Access. (2024).
[4] P.H. Hoang, G. Ozkan, P.R. Badr, B. Papari, C.S. Edrington, M.A. Zehir, B. Hayes, L. Mehigan, D.Al Kez, A.M. Foley, A dual distributed optimal energy management method for distribution grids with electric vehicles, IEEE Trans. Intell. Transp. Syst. 23 (8) (2021) 13 666–13 677.
[5] C.L. Bhattar, M.A. Chaudhari, Centralized energy management scheme for grid connected dc microgrid, IEEE Syst. J. 17 (3) (2023) 3741–3751.
[6] C. Samende, S.M. Bhagavathy, M. McCulloch, Distributed state of charge-based droop control algorithm for reducing power losses in multiport converter-enabled solar dc nano-grids, IEEE Trans. Smart Grid 12 (6) (2021) 4584–4594.
[7] B. Papari, C.S. Edrington, I. Bhattacharya, G. Radman, Effective energy management of hybrid ac–dc microgrids with storage devices, IEEE Trans. smart grid 10 (1) (2017) 193–203.
[8] P.Teimourzadeh Baboli, M. Shahparasti, M. Parsa Moghaddam, M.R. Haghifam, M. Mohamadian, Energy management and operation modelling of hybrid ac–dc microgrid, IET Gener. Transm. & Distrib. 8 (10) (2014) 1700–1711.
[9] S. Moradi, G.D.A. Tinajero, J.C. Vasquez, G. Zizzo, J.M. Guerrero, E.R. Sanseverino, Hierarchical-power-flow-based energy management for alternative/direct current hybrid microgrids, Sustainable Energy, Grids Netw. 38 (2024) 101384.
[10] X. Liu, Y. Wang, X. Liu, T. Zhao, P. Wang, More efficient energy management for hybrid ac/dc microgrids with hard constrained neural network-based conversion loss surrogate models, IEEE Trans. Smart Grid (2023).
[11] T. Zhao, X. Liu, P. Wang, F. Blaabjerg, More efficient energy management for networked hybrid ac/dc microgrids with multivariable nonlinear conversion losses, IEEE Sys. J. 17 (2) (2022) 3212–3223.
[12] S. Paul, A. Sharma, N.P. Padhy, Risk constrained energy efficient optimal operation of a converter governed ac/dc hybrid distribution network with distributed energy resources and volt-var controlling devices, IEEE Trans. Ind. Appl. 57 (4) (2021) 4263–4277.
[13] Z. Liang, H. Chen, X. Wang, S. Chen, C. Zhang, Risk-based uncertainty set optimization method for energy management of hybrid ac/dc microgrids with uncertain renewable generation, IEEE Trans. Smart Grid 11 (2) (2019) 1526–1542.
[14] S. Moradi, G. Zizzo, S. Favuzza, F. Massaro, A stochastic approach for self-healing capability evaluation in active islanded ac/dc hybrid microgrids, Sustainable Energy, Grids Netw. 33 (2023) 100982.
[15] F. Marasciuolo, M. Dicorato, G. Tricarico, P. Montegiglio, G. Forte, M. Trovato, The influence of ev usage scenarios on dc microgrid technoeconomic operation, IEEE Trans. Ind. Appl. 58 (3) (2022) 3957–3966.
[16] F. Marasciuolo, C. Orozco, M. Dicorato, A. Borghetti, G. Forte, Chance-constrained calculation of the reserve service provided by ev charging station clusters in energy communities, IEEE Trans. Ind. Appl. 59 (4) (2023) 4700–4709.
[17] H. Shaker, H. Zareipour, D. Wood, A data-driven approach for estimating the power generation of invisible solar sites, IEEE Trans. Smart Grid 7 (5) (2015) 2466–2476.
[18] J. Lin, J. Ma, J. Zhu, A privacy-preserving federated learning method for probabilistic community-level behind-the-meter solar generation disaggregation, IEEE Trans. Smart Grid 13 (1) (2021) 268–279.
[19] F. Bu, R. Cheng, Z. Wang, A two-layer approach for estimating behind-the-meter pv generation using smart meter data, IEEE Trans. Power Syst. 38 (1) (2022) 885–896.
[20] R. Saeedi, S.K. Sadanandan, A.K. Srivastava, K.L. Davies, A.H. Gebremedhin, An adaptive machine learning framework for behindthe- meter load/pv disaggregation, IEEE Trans. Ind. Inform. 17 (10) (2021) 7060–7069.
[21] X. Fu, C. Zhang, Y. Xu, Y. Zhang, H. Sun, Statistical machine learning for power flow analysis considering the influence of weather factors on photovoltaic power generation, IEEE Trans. Neural Netw. Learn. Syst. (2024).
[22] J. Yuan, Y. Weng, Enhance unobservable solar generation estimation via constructive generative adversarial networks, IEEE Trans. Power Syst. 39 (1) (2023) 2251–2263.
[23] Y. Li, R. Wang, Z. Yang, Optimal scheduling of isolated microgrids using automated reinforcement learning-based multi-period forecasting, IEEE Trans. Sustain. Energy 13 (1) (2021) 159–169.
[24] N. Mahdavi, D. Weeraddana, Y. Guo, Probabilistic estimation of pv generation at customer and distribution feeder levels using net-demand data, IEEE Trans. Smart Grid 14 (3) (2022) 1974–1984.
[25] H. Dui, Y. Zhang, X. Wu, L. Xing, Dynamic reliability assessment model for iot-enabled smart offshore wind farm, IEEE Trans. Rel (2024).
[26] X. Zhan, L. Kou, M. Xue, J. Zhang, L. Zhou, Reliable long-term energy load trend prediction model for smart grid using hierarchical decomposition self-attention network, IEEE Trans. Rel 72 (2) (2022) 609–621.
[27] S. Sahoo, S. Mishra, A multi-objective adaptive control framework in autonomous dc microgrid, IEEE Trans. Smart Grid 9 (5) (2017) 4918–4929.
[28] Q. Zhao, K. Liao, J. Yang, Z. He, Y. Xu, Aging rate equalization strategy for battery energy storage systems in microgrids, IEEE Trans. Smart Grid 15 (1) (2023) 136–148.
[29] H. Mahmood, F. Blaabjerg, Autonomous power management of distributed energy storage systems in islanded microgrids, IEEE Trans. Sustain. Energy 13 (3) (2022) 1507–1522.
[30] W. Kang, M. Chen, Y. Guan, L. Tang, J.M. Guerrero, et al., Distributed event-triggered optimal control method for heterogeneous energy storage systems in smart grid, IEEE Trans. Sustain. Energy 13 (4) (2022) 1944–1956.
[31] B. Huang, S. Zheng, R. Wang, H. Wang, J. Xiao, P. Wang, Distributed optimal control of dc microgrid considering balance of charge state, IEEE Trans. Energy Convers. 37 (3) (2022) 2162–2174.
[32] H.W. Yan, A. Narang, H.D. Tafti, G.G. Farivar, S. Ceballos, J. Pou, Minimizing energy storage utilization in a stand-alone dc microgrid using photovoltaic flexible power control, IEEE Trans. Smart Grid 12 (5) (2021) 3755–3764.
[33] H.W. Yan, G.G. Farivar, N. Beniwal, H.D. Tafti, S. Ceballos, J. Pou, G. Konstantinou, Battery lifetime extension in a stand-alone microgrid with flexible power point tracking of photovoltaic system, IEEE J. Emerg. Sel. Top. Power Electron. 11 (2) (2022) 2281–2290.
[34] D.M. Yehia, M. Numair, D.-E.A. Mansour, A novel iot-based droop control for battery soc balancing among multiple microgrids, IEEE Trans. Smart Grid (2023).
[35] T.A. Fagundes, G.H.F. Fuzato, L.J.R. Silva, A.M. dos Santos Alonso, J.C. Vasquez, J. M. Guerrero, R.Q. Machado, Battery energy storage systems in microgrids: A review of soc balancing and perspectives, IEEE Open. J. Ind. Electron. Soc. 5 (2024) 961–992.
[36] S.O. Kimbrough and H.U.¨mitcan Yilmaz, A symmetric block resampling method to generate energy time series data, in 2021 22nd IEEE International Conference on Industrial Technology (ICIT), 2021.
[37] J. Usaola, Synthesis of hourly wind power series using the moving block bootstrap method, in 2014 International Conference on Probabilistic Methods Applied to Power Systems (PMAPS), 2014.
[38] S. Moradi, G. Zizzo, S. Favuzza, F. Massaro, A stochastic approach for self-healing capability evaluation in active islanded ac/dc hybrid microgrids, Sustainable Energy, Grids Netw. 33 (2023) 100982.

[39] S. Favuzza, M.G. Ippolito, F. Massaro, S. Moradi, R. Musca, V. Porgi, G. Zizzo, G. Adinolfi, A. Ricca, R. Ciavarella et al., Dynamic control of static converters for the transition from grid-on to grid-off operation of ac/dc microgrids, in 2022 IEEE International Conference on Environment and Electrical Engineering and 2022 IEEE Industrial and Commercial Power Systems Europe (EEEIC/I&CPS Europe). IEEE, 2022, pp. 1–6.

[40] A. Bon`ı, S. Favuzza, M.G. Ippolito, F. Massaro, S. Modari, R. Musca, V. Porgi, and G. Zizzo, A simulation analysis for assessing the reliability of ac/dc hybrid microgrids–part i: Underground station and car parking, in 2021 IEEE International Conference on Environment and Electrical Engineering and 2021 IEEE Industrial and Commercial Power Systems Europe (EEEIC/I&CPS Europe). IEEE, 2021, pp. 1–6.

[41] A. Bon`ı, S. Favuzza, M.G. Ippolito, F. Massaro, S. Moradi, R. Musca, V. Porgi, and G. Zizzo, A simulation analysis for assessing the reliability of ac/dc hybrid microgrids–part ii: Port area and residential area, in 2021 IEEE International Conference on Environment and Electrical Engineering and 2021 IEEE Industrial and Commercial Power Systems Europe (EEEIC/I&CPS Europe). IEEE, 2021, pp. 1–6.

[42] S.O. Kimbrough and H.U.¨mitcan Yilmaz, A symmetric block resampling method to generate energy time series data, in 2021 22nd IEEE International Conference on Industrial Technology (ICIT), 2021.

[43] J. Usaola, Synthesis of hourly wind power series using the moving block bootstrap method, in 2014 International Conference on Probabilistic Methods Applied to Power Systems (PMAPS), 2014.